

Neutrino Masses and Heavy Triplet Leptons at the LHC: Testability of Type III Seesaw

Tong Li¹, Xiao-Gang He^{1,2}

¹*Center for High Energy Physics, Peking University, Beijing, 100871*

²*Department of Physics and Center for Theoretical Sciences, National Taiwan University, Taipei*

(Dated: July 4, 2018)

We study LHC signatures of Type III seesaw in which $SU(2)_L$ triplet leptons are introduced to supply the heavy seesaw masses. To detect the signals of these heavy triplet leptons, one needs to understand their decays to standard model particles which depend on how light and heavy leptons mix with each other. We concentrate on the usual solutions with small light and heavy lepton mixing of order the square root of the ratio of light and heavy masses, $(m_\nu/M_{\nu_R})^{1/2}$. This class of solutions can lead to a visible displaced vertex detectable at the LHC which can be used to distinguish small mixing and large mixing between light and heavy leptons. We show that, in this case, the couplings of light and heavy triplet leptons to gauge and Higgs bosons, which determine the decay widths and branching ratios, can be expressed in terms of light neutrino masses and their mixing. Using these relations, we study heavy triplet lepton decay patterns and production cross section at the LHC. If these heavy triplet leptons are below a TeV or so, they can be easily produced at the LHC due to their gauge interactions from being non-trivial representations of $SU(2)_L$. We consider two ideal production channels, 1) $E^+E^- \rightarrow \ell^+\ell^+\ell^-\ell^-jj$ ($\ell = e, \mu, \tau$) and 2) $E^\pm N \rightarrow \ell^\pm\ell^\pm jjjj$ in detail. For case 1), we find that with one or two of the light leptons being τ it can also be effectively studied. With judicious cuts at the LHC, the discovery of the heavy triplet leptons as high as a TeV can be achieved with $100fb^{-1}$ integrated luminosity.

I. INTRODUCTION

Neutrino oscillation experiments involving neutrinos and antineutrinos coming from astrophysical and terrestrial sources have found compelling evidence that neutrinos have finite but small masses. To accommodate this observation, the minimal standard model (SM) must be extended. Generating neutrino masses through the seesaw mechanism [1, 2, 3, 4] is among the most attractive ones. It explains the smallness of neutrino mass by supplying a suppression factor of the ratio of electroweak scale to a new physics scale. There are different ways to realize seesaw mechanism. They can be categorized as Type I, Type II and Type III seesaw mechanisms. The main ingredients of these models are as the followings.

Type I [1]: Introducing singlet right-handed neutrinos ν_R which transform as: $(1, 1, 0)$ under SM $SU(3)_C \times SU(2)_L \times U(1)_Y$ gauge group. It is clear that ν_R does not have SM gauge interactions. The

neutrino masses m_ν are given by $m_\nu \sim y_\nu^2 v^2 / M_{\nu_R}$, where v is the vacuum expectation value (vev) of the Higgs doublet in the SM, y_ν is the Yukawa coupling and M_{ν_R} is the right-handed neutrino mass, which sets the new physics scale Λ . If $y_\nu \simeq 1$, to obtain the light neutrino mass of order an eV or smaller, M_{ν_R} is required to be of order $10^{14} \sim 10^{15}$ GeV. This makes it impossible to directly detect ν_R at laboratory experiment. However, the Yukawa coupling y_ν does not need to be of order one. If it turns out to be similar to or smaller than the Yukawa coupling for electron, M_{ν_R} can be as low as a TeV.

Type II [2]: Introducing a triplet Higgs representation Δ transforming as: $(1, 3, 2)$. In this type of models, the neutrino masses are given by: $m_\nu \approx Y_\nu v_\Delta$, where v_Δ is the vev of the neutral component of the triplet and Y_ν is the Yukawa coupling. With a doublet and triplet mixing via a dimensionful parameter μ , the electroweak symmetry breaking (EWSB) leads to a relation $v_\Delta \sim \mu v^2 / M_\Delta^2$, where M_Δ is the mass of the triplet. In this case the scale Λ is replaced by M_Δ^2 / μ . With $Y_\nu \approx 1$ and $\mu \sim M_\Delta$, the scale Λ is also $10^{14} \sim 10^{15}$ GeV. Again a lower value of order a TeV for M_Δ is possible.

Type III [3]: Introducing triplet lepton representations Σ_L with $(1, 3, 0)$ SM quantum numbers. The resulting mass matrix for neutrinos has the same form as that in Type I seesaw. The high scale Λ is replaced by the mass of the leptons in the $SU(2)_L$ triplet representation which can also be as low as a TeV.

In the absence of more experimental data, it is impossible to tell which, if any, of the mechanisms is actually correct. Different models should be studied using available data or future ones. The most direct way of verifying the seesaw mechanism is, of course, to produce the heavy degrees of freedom in the models if they are light enough, and study their properties. The Large Hadron Collider (LHC) at CERN with the unprecedented high energy and luminosity is the best place to carry out such a test.

Major discoveries of exciting new physics at the Terascale at the LHC are highly anticipated. Test of seesaw mechanism at LHC has received a lot of attentions recently [5, 6, 7, 8, 9, 10, 11, 12, 13]. However, it is believed that any signal of ν_R would indicate a more subtle mechanism beyond the simple Type I seesaw due to the otherwise naturally small mixing $V_{\nu_R} \sim \sqrt{m_\nu / M_{\nu_R}}$ between the heavy neutrinos and the SM leptons. Some of the ways to evade such a situation are to have some new gauge interactions [6, 8] or to find solutions where V_{ν_R} are large which can happen in inverse seesaw models [14, 15, 16].

The possibility of testing the Type II seesaw mechanism at the LHC has been considered by several groups [9, 10]. Recently one group including one of us systematically explored the parameter space in this model [10]. Using preferred parameters from experimental data, they found that in the optimistic scenarios, by identifying the flavor structure of the lepton number violating decays of the charged Higgs bosons, one can establish the neutrino mass pattern of the normal hierarchy (NH), inverted hierarchy (IH) or quasi-degenerate (QD). Many other signatures of Type II seesaw at the LHC have been studied [9, 10].

There have also been studies to test Type III seesaw at the LHC [11, 12, 13]. Due to the fact that the

$SU(2)_L$ triplet Σ has gauge interactions, the production of the heavy triplet particles can have a much larger cross section compared with that in Type I seesaw. The Type III seesaw can be tested in a more comprehensive way up to the TeV range. In this paper we further study some features of the Type III seesaw at LHC. To detect the signals of the heavy triplet leptons, one needs to understand their decays to SM particles which depend on how light and heavy leptons mix with each other. Similar to Type-I seesaw, in this model it is also possible to have small and large mixing $V_{l\nu_R}$ between light and heavy leptons [14, 15, 16].

The usual solutions with light and heavy lepton mixing of order the square root of the ratio of light and heavy masses, $(m_\nu/M_{\nu_R})^{1/2}$ could lead to a visible displaced vertex in the detector at the LHC [11]. This fact can be used to distinguish small mixing and large mixing between light and heavy leptons. The latter does not lead to a displaced vertex. It has long been realized that it is possible to have large light and heavy neutrino mixing originated from the so-called inverse seesaw [14]. This possibility has also received a lot of attentions recently [15, 16]. With a large mixing between light and heavy leptons, one can also study single heavy lepton production [16]. This can also be used to distinguish model parameter spaces. We will concentrate on the usual small light and heavy mixing solutions.

The analysis carried out in this work, in many ways, is similar to that in Ref. [8] since in both cases the productions of heavy lepton pairs are through gauge boson mediation, and also the light and heavy lepton mixing comes from seesaw mechanism. The main differences are that in this model the heavy leptons have electroweak interactions and the mediating gauge bosons in productions are W and Z , while in the model discussed in Ref. [8], the heavy neutrinos do not have electroweak interactions and the mediating particle is the new neutral gauge boson Z' . Our analysis also has overlaps with that in Ref. [17] where Type I+III seesaw was studied, but detailed correlations are different since the model in Ref. [17] has both heavy neutrinos from Type I which do not have electroweak interactions and also the triplet heavy leptons from Type III we are considering. We have checked that when applicable, our results agree with those obtained in Ref. [8, 17].

We find that there is a relation between the low energy neutrino oscillation and mass parameters, and the heavy triplet lepton decay parameters which has not been considered before in this model. We first derive this relation, and then make concrete predictions of the heavy triplet lepton signals using this relation for the small mixing solutions. We consider two ideal production channels, 1) $E^+E^- \rightarrow \ell^+\ell^+\ell^-\ell^-jj$ ($\ell = e, \mu, \tau$) and 2) $E^\pm N \rightarrow \ell^\pm\ell^\pm jjjj$ in detail. We also include τ events reconstruction in the analysis which turns out to give some interesting additional information. With judicious cuts at the LHC, the discovery of the heavy triplet leptons as high as a TeV can be achieved with $100fb^{-1}$ integrated luminosity. With $300fb^{-1}$ integrated luminosity, the reach of the scale for heavy triplet leptons can be higher.

The paper is arranged as the following. In Sec. II we summarize some basic features of Type III seesaw

model, paying particular attention to the heavy triplet lepton couplings to SM bosons and light leptons, and display relations between the low energy neutrino oscillation and mass parameters. In Sec. III we study constraints on the relevant parameters in the model, taking full advantage of the relations obtained in Sec. II. In Sec. IV we study the heavy triplet lepton decays. In Sec. V we study production of heavy triplet leptons and the detection signals at the LHC. Finally in Sec. VI we summarize our main results. We also include two appendices, Appendix A and Appendix B, to provide more details on the derivation of the relation displayed in Sec. II and the general expressions for the heavy triplet lepton decay parameters.

II. THE TYPE III SEESAW MODEL

The Type III seesaw model consists, in addition to the SM particles, left-handed triplet leptons with zero hypercharge, $\Sigma_L \sim (1, 3, 0)$ under $SU(3)_C \times SU(2)_L \times U(1)_Y$ [3]. We write the component fields as

$$\Sigma_L = \begin{pmatrix} \Sigma_L^0/\sqrt{2} & \Sigma_L^+ \\ \Sigma_L^- & -\Sigma_L^0/\sqrt{2} \end{pmatrix}. \quad (1)$$

The charge conjugated form is

$$\Sigma_L^c = \begin{pmatrix} \Sigma_L^{0c}/\sqrt{2} & \Sigma_L^{-c} \\ \Sigma_L^{+c} & -\Sigma_L^{0c}/\sqrt{2} \end{pmatrix}. \quad (2)$$

Note that Σ_L^c is right-handed.

The renormalizable Lagrangian involving $\Sigma_L(\Sigma_L^c)$ is given by

$$\mathcal{L} = \text{Tr}[\overline{\Sigma}_L i \not{D} \Sigma_L] - \frac{1}{2} \text{Tr}[\overline{\Sigma}_L^c M_\Sigma \Sigma_L + \overline{\Sigma}_L M_\Sigma^* \Sigma_L^c] - \overline{L}_L \sqrt{2} Y_\Sigma^\dagger \Sigma_L^c \tilde{H} - \tilde{H}^\dagger \overline{\Sigma}_L^c \sqrt{2} Y_\Sigma L_L. \quad (3)$$

Here we have defined that $\Psi \equiv \Sigma_L^- + \Sigma_L^{+c}$ with $\Psi_L = \Sigma_L^-$, $\Psi_R = \Sigma_L^{+c}$. In the above $L_L \sim (1, 2, -1)$ is the left-handed doublet lepton field, and $\tilde{H} = i\sigma_2 H^* \sim (1, 2, -1)$ is the Higgs doublet field.

With a non-zero vacuum expectation value $\langle H \rangle = v/\sqrt{2}$ for the Higgs field, the doublet leptons receive masses, and also mix the doublet and triplet leptons. The relevant terms in the Lagrangian for mass matrices are given by

$$\begin{aligned} \mathcal{L}_m = & - \left(\overline{l}_R \quad \overline{\Psi}_R \right) \begin{pmatrix} m_l & 0 \\ Y_\Sigma v & M_\Sigma \end{pmatrix} \begin{pmatrix} l_L \\ \Psi_L \end{pmatrix} + h.c. \\ & - \left(\overline{\nu}_L^c \quad \overline{\Sigma}_L^{0c} \right) \begin{pmatrix} 0 & Y_\Sigma^T v/2\sqrt{2} \\ Y_\Sigma v/2\sqrt{2} & M_\Sigma/2 \end{pmatrix} \begin{pmatrix} \nu_L \\ \Sigma_L^0 \end{pmatrix} + h.c. \end{aligned} \quad (4)$$

The second line above gives the seesaw mass matrix for neutrinos.

There are many different features for Type III seesaw compared with the other types. Unlike Type I seesaw model, in this model the doublet charged leptons mix with the triplet charged leptons leading to tree level flavor changing neutral current involving charged leptons [18]. The fact that the heavy triplet leptons in Type III seesaw have gauge interaction also leads to other different phenomenology [19, 20]. Different extensions of the simplest model can also achieve different goals [21].

For detailed studies, one needs to understand the mass matrices in Eq. 4 and their diagonalization further. The diagonalization of the mass matrices can be achieved by making unitary transformations on the triplet, the charged and neutral, leptons defined in the following

$$\begin{pmatrix} l_{L,R} \\ \Psi_{L,R} \end{pmatrix} = U_{L,R} \begin{pmatrix} l_{mL,R} \\ \Psi_{mL,R} \end{pmatrix}, \quad \begin{pmatrix} \nu_L \\ \Sigma_L^0 \end{pmatrix} = U_0 \begin{pmatrix} \nu_{mL} \\ \Sigma_{mL}^0 \end{pmatrix}, \quad (5)$$

where $U_{L,R}$ and U_0 are 6×6 unitary matrices, for 3 light doublet and 3 heavy triplet lepton fields, which we decompose into 3×3 block matrices as

$$U_L \equiv \begin{pmatrix} U_{Lll} & U_{Ll\Psi} \\ U_{L\Psi l} & U_{L\Psi\Psi} \end{pmatrix}, \quad U_R \equiv \begin{pmatrix} U_{Rll} & U_{Rl\Psi} \\ U_{R\Psi l} & U_{R\Psi\Psi} \end{pmatrix}, \quad U_0 \equiv \begin{pmatrix} U_{0\nu\nu} & U_{0\nu\Sigma} \\ U_{0\Sigma\nu} & U_{0\Sigma\Sigma} \end{pmatrix}. \quad (6)$$

For our studies we need to know gauge and Higgs boson couplings to leptonic fields. In the weak interaction basis, they can be written as

$$\begin{aligned} \mathcal{L}_{gauge} &= +e(\bar{\Psi}\gamma^\mu\Psi + \bar{l}\gamma^\mu l)A_\mu + gc_W(\bar{\Psi}\gamma^\mu\Psi + \bar{l}\gamma^\mu l)Z_\mu \\ &- \frac{g}{c_W}(\frac{1}{2}\bar{\nu}_L\gamma^\mu\nu_L + \frac{1}{2}\bar{l}_L\gamma^\mu l_L + \bar{l}_R\gamma_\mu l_R)Z_\mu \\ &- g(\bar{\Psi}_L\gamma^\mu\Sigma_L^0 W_\mu^- + \bar{\Psi}_R\gamma^\mu\Sigma_L^{0c}W_\mu^-) - \frac{g}{\sqrt{2}}\bar{l}_L\gamma^\mu\nu_L W_\mu^- + h.c., \\ \mathcal{L}_{Yukawa} &= -(\bar{\nu}_L Y_\Sigma^\dagger \Sigma_L^{0c} + \sqrt{2}\bar{l}_L Y_\Sigma^\dagger \Psi_R) \frac{H^0}{\sqrt{2}} - \bar{l}_R m_l l_L \frac{H^0}{v} + h.c., \end{aligned} \quad (7)$$

where $c_W = \cos \theta_W$.

In the mass eigen-state basis, the photon couplings to fermions are diagonal, but Z couplings are more complicated. We have

$$\mathcal{L}_{NCZ} \equiv \mathcal{L}_{NCZ}^A + \mathcal{L}_{NCZ}^B + (\mathcal{L}_{NCZ}^C + h.c.) + (\mathcal{L}_{NCZ}^D + h.c.) + \mathcal{L}_{NCZ}^E + \mathcal{L}_{NCZ}^F \quad (8)$$

where

$$\begin{aligned}
\mathcal{L}_{NCZ}^A &= g_{cW} [\overline{\Psi}_m V_{Z\Psi}^L \gamma^\mu P_L \Psi_{m'} Z_\mu^0 + \overline{\Psi}_m V_{Z\Psi}^R \gamma^\mu P_R \Psi_{m'} Z_\mu^0], \\
\mathcal{L}_{NCZ}^B &= -\frac{g}{2c_W} \overline{\Sigma}_{mL}^0 V_{Z\Sigma}^L \gamma^\mu P_L \Sigma_{m'L}^0 Z_\mu^0, \\
\mathcal{L}_{NCZ}^C &= \frac{g}{2c_W} \overline{\nu}_m V_{Z\nu\Sigma}^L \gamma^\mu P_L \Sigma_{m'L}^0 Z_\mu^0, \\
\mathcal{L}_{NCZ}^D &= \frac{g}{\sqrt{2}c_W} [\overline{l}_m V_{Zl\Psi}^L \gamma^\mu P_L \Psi_{m'} Z_\mu^0 + \overline{l}_m V_{Zl\Psi}^R \gamma^\mu P_R \Psi_{m'} Z_\mu^0], \\
\mathcal{L}_{NCZ}^E &= -\frac{g}{2c_W} \overline{\nu}_m V_{Z\nu\nu}^L \gamma^\mu P_L \nu_{m'} Z_\mu^0, \\
\mathcal{L}_{NCZ}^F &= -\frac{g}{c_W} [\overline{l}_m V_{Zl}^L \gamma^\mu P_L l_{m'} Z_\mu^0 + \overline{l}_m V_{Zl}^R \gamma^\mu P_R l_{m'} Z_\mu^0],
\end{aligned} \tag{9}$$

and

$$\begin{aligned}
V_{Z\Psi}^L &= I - \frac{1}{2c_W^2} U_{Ll\Psi}^\dagger U_{Ll\Psi}, \quad V_{Z\Psi}^R = I - \frac{1}{c_W^2} U_{Rl\Psi}^\dagger U_{Rl\Psi}, \quad V_{Z\Sigma\Sigma}^L = U_{0\nu\Sigma}^\dagger U_{0\nu\Sigma}, \\
V_{Z\nu\Sigma}^L &= -U_{0\nu\nu}^\dagger U_{0\nu\Sigma}, \quad V_{Zl\Psi}^L = -\frac{1}{\sqrt{2}} U_{Ll}^\dagger U_{Ll\Psi}, \quad V_{Zl\Psi}^R = -\sqrt{2} U_{Rl}^\dagger U_{Rl\Psi}, \\
V_{Z\nu\nu}^L &= U_{0\nu\nu}^\dagger U_{0\nu\nu}, \quad V_{Zll}^L = -c_W^2 I + \frac{1}{2} U_{Ll}^\dagger U_{Ll}, \quad V_{Zll}^R = -c_W^2 I + U_{Rl}^\dagger U_{Rl}.
\end{aligned}$$

For the charged current interactions, we have

$$\mathcal{L}_{CC} \equiv (\mathcal{L}_{CC}^A + \mathcal{L}_{CC}^B + \mathcal{L}_{CC}^C + \mathcal{L}_{CC}^D + h.c.) \tag{10}$$

where

$$\begin{aligned}
\mathcal{L}_{CC}^A &= -\frac{g}{\sqrt{2}} [\overline{\Psi}_m V_{\Psi\Sigma}^L \gamma^\mu P_L \Sigma_{m'L}^0 W_\mu^- + \overline{\Psi}_m V_{\Psi\Sigma}^R \gamma^\mu P_R \Sigma_{m'L}^{0c} W_\mu^-], \\
\mathcal{L}_{CC}^B &= -\frac{g}{\sqrt{2}} [\overline{l}_m V_{l\Sigma}^L \gamma^\mu P_L \Sigma_{m'L}^0 W_\mu^- + \overline{l}_m V_{l\Sigma}^R \gamma^\mu P_R \Sigma_{m'L}^{0c} W_\mu^-], \\
\mathcal{L}_{CC}^C &= -\frac{g}{\sqrt{2}} [\overline{\Psi}_m V_{\Psi\nu}^L \gamma^\mu P_L \nu_{m'L} W_\mu^- + \overline{\Psi}_m V_{\Psi\nu}^R \gamma^\mu P_R \nu_{m'L}^c W_\mu^-], \\
\mathcal{L}_{CC}^D &= -\frac{g}{\sqrt{2}} [\overline{l}_m V_{l\nu}^L \gamma^\mu P_L \nu_{m'L} W_\mu^- + \overline{l}_m V_{l\nu}^R \gamma^\mu P_R \nu_{m'L}^c W_\mu^-],
\end{aligned} \tag{11}$$

and

$$\begin{aligned}
V_{\Psi\Sigma}^L &= U_{Ll\Psi}^\dagger U_{0\nu\Sigma} + \sqrt{2} U_{L\Psi\Psi}^\dagger U_{0\Sigma\Sigma}, \quad V_{\Psi\Sigma}^R = \sqrt{2} U_{R\Psi\Psi}^\dagger U_{0\Sigma\Sigma}^*, \\
V_{l\Sigma}^L &= U_{Ll}^\dagger U_{0\nu\Sigma} + \sqrt{2} U_{L\Psi l}^\dagger U_{0\Sigma\Sigma}, \quad V_{l\Sigma}^R = \sqrt{2} U_{R\Psi l}^\dagger U_{0\Sigma\Sigma}^*, \\
V_{\Psi\nu}^L &= U_{Ll\Psi}^\dagger U_{0\nu\nu} + \sqrt{2} U_{L\Psi\Psi}^\dagger U_{0\Sigma\nu}, \quad V_{\Psi\nu}^R = \sqrt{2} U_{R\Psi\Psi}^\dagger U_{0\Sigma\nu}^*, \\
V_{l\nu}^L &\equiv V_{PMNS} = U_{Ll}^\dagger U_{0\nu\nu} + \sqrt{2} U_{L\Psi l}^\dagger U_{0\Sigma\nu}, \quad V_{l\nu}^R = \sqrt{2} U_{R\Psi l}^\dagger U_{0\Sigma\nu}^*.
\end{aligned} \tag{12}$$

In the above we have made the approximation $V_{l\nu}^L = V_{PMNS}$. Strictly speaking $V_{l\nu}^L$ is not unitary as the usual definition of the unitary 3×3 V_{PMNS} matrix. The correction is at the order of $\mathcal{O}(m_\nu/M_\Sigma)$. It is a good approximation since we are working with the small light and heavy neutrino mixing scenario.

One finds an interesting relation

$$V_{l\Sigma}^{L*} M_{\Sigma N}^{diag} V_{l\Sigma}^{L\dagger} = -V_{PMNS}^* m_\nu^{diag} V_{PMNS}^\dagger + m_l^{diag} U_{R\Psi l}^T U_{L\Psi l} + U_{L\Psi l}^T U_{R\Psi l} m_l^{diag} . \quad (13)$$

The detailed derivation is given in Appendix A. A similar relation without the last two terms on the right in the above equation for Type I seesaw has been derived in Ref. [8, 22].

The physical Higgs H^0 interactions with leptonic fields, in the mass eigen-state basis, are given by

$$\mathcal{L}_S \equiv \mathcal{L}_S^A + \mathcal{L}_S^B + h.c. , \quad (14)$$

where

$$\begin{aligned} \mathcal{L}_S^A &= -\overline{\nu}_m V_{S\nu\Sigma}^R P_R \Sigma_{m'L}^{0c} H^0 , \\ \mathcal{L}_S^B &= -[\overline{l}_m V_{Sl\Psi}^L P_L \Psi_{m'} + \overline{l}_m V_{Sl\Psi}^R P_R \Psi_{m'}] H^0 , \end{aligned} \quad (15)$$

and

$$\begin{aligned} V_{S\nu\Sigma}^R &= [U_{0\nu\nu}^\dagger Y_\Sigma^\dagger U_{0\Sigma\Sigma}^* + U_{0\Sigma\nu}^\dagger Y_\Sigma^* U_{0\nu\Sigma}^*] / \sqrt{2} , \\ V_{Sl\Psi}^L &= U_{R\Psi l}^\dagger Y_\Sigma U_{Ll\Psi} + \frac{1}{\sqrt{2}v} U_{Lll}^\dagger m_l U_{Rl\Psi} , \quad V_{Sl\Psi}^R = U_{Lll}^\dagger Y_\Sigma^\dagger U_{R\Psi\Psi} + \frac{1}{\sqrt{2}v} U_{Rll}^\dagger m_l U_{Ll\Psi} . \end{aligned} \quad (16)$$

In principle, the matrices $U_{L,R}$ and U_0 can be expressed in terms of Y_Σ , m_l and M_Σ . Since for seesaw mechanism to work, $Y_\Sigma v M_\Sigma^{-1}$ should be small, one can expand $U_{L,R}$ and U_0 in powers of $Y_\Sigma v M_\Sigma^{-1}$ to keep track of the leading order contributions. For this purpose, it is convenient to write the leading order expressions up to $Y_\Sigma^2 v^2 M_\Sigma^{-2}$ in the basis where m_l and M_Σ are already diagonalized, without loss of generality. The following results have been obtained in the literature [18]

$$\begin{aligned} U_{Lll} &= 1 - \epsilon , \quad U_{Ll\Psi} = Y_\Sigma^\dagger M_\Sigma^{-1} v , \quad U_{L\Psi l} = -M_\Sigma^{-1} Y_\Sigma v , \quad U_{L\Psi\Psi} = 1 - \epsilon' , \\ U_{Rll} &= 1 , \quad U_{Rl\Psi} = m_l Y_\Sigma^\dagger M_\Sigma^{-2} v , \quad U_{R\Psi l} = -M_\Sigma^{-2} Y_\Sigma m_l v , \quad U_{R\Psi\Psi} = 1 , \\ U_{0\nu\nu} &= (1 - \epsilon/2) V_{PMNS} , \quad U_{0\nu\Sigma} = Y_\Sigma^\dagger M_\Sigma^{-1} v / \sqrt{2} , \quad U_{0\Sigma\nu} = -M_\Sigma^{-1} Y_\Sigma U_{0\nu\nu} v / \sqrt{2} , \\ U_{0\Sigma\Sigma} &= 1 - \epsilon'/2 , \quad \epsilon = Y_\Sigma^\dagger M_\Sigma^{-2} Y_\Sigma v^2 / 2 , \quad \epsilon' = M_\Sigma^{-1} Y_\Sigma Y_\Sigma^\dagger M_\Sigma^{-1} v^2 / 2 . \end{aligned}$$

To leading order in $Y_\Sigma v M_\Sigma^{-1}$, we have interaction terms involving heavy triplet leptons as

$$\begin{aligned} \mathcal{L}_{NC(A+Z)} &= e \overline{E} \gamma^\mu E A_\mu + g_{cW} \overline{E} \gamma^\mu E Z_\mu^0 , \\ \mathcal{L}_{NCZ} &= \frac{g}{2c_W} [\overline{\nu} (V_{PMNS}^\dagger V_{lN} \gamma^\mu P_L - V_{PMNS}^T V_{lN}^* \gamma^\mu P_R) N + \sqrt{2} \overline{l} V_{lN} \gamma^\mu P_L E + h.c.] Z_\mu^0 , \\ \mathcal{L}_{CC} &= -g [\overline{E} \gamma^\mu N + \frac{1}{\sqrt{2}} \overline{l} V_{lN} \gamma^\mu P_L N + \overline{E} V_{lN}^T V_{PMNS}^* \gamma^\mu P_R \nu] W_\mu^- + h.c. , \\ \mathcal{L}_S &= \frac{g}{2M_W} [\overline{\nu} (V_{PMNS}^\dagger V_{lN} M_N^{diag} P_R + V_{PMNS}^T V_{lN}^* M_N^{diag} P_L) N + \sqrt{2} \overline{l} V_{lN} M_E^{diag} P_R E] H^0 + h.c. , \end{aligned} \quad (17)$$

with $V_{lN} \equiv V_{l\Sigma}^L = -Y_\Sigma^\dagger v M_\Sigma^{-1} / \sqrt{2}$. In the above, all fields are in mass eigen-states. The E , N and M_E^{diag}, M_N^{diag} are mass eigen-states of Ψ , Σ , and the eigen-mass matrices, respectively. Note that the interactions involving light neutrinos in the above have the additional V_{PMNS} factor compared with those involving light charged leptons.

To the same order, we also have

$$V_{lN}^* M_N^{diag} V_{lN}^\dagger = -V_{PMNS}^* m_\nu^{diag} V_{PMNS}^\dagger. \quad (18)$$

This equation plays an important role in constraining the elements in the coupling matrix V_{lN} .

III. CONSTRAINTS ON THE PHYSICAL PARAMETERS

In the study of decay of E and N into SM particles, the interaction matrix V_{lN} plays an important role. Knowledge about it is crucial. In this section we study constraints on V_{lN} and the decay branching ratios of E and N . Eq. 18 provides very important constraints on V_{lN} . As have been mentioned before that there are two classes of solutions, the cases with small and large mixing between light and heavy leptons. The small mixing case is characterized by the fact that in the limit, m_ν^{diag} goes to zero, the elements in V_{lN} also go to zero, and the elements in V_{lN} are of order $(m_\nu/M_{\nu_R})^{1/2}$. But with more than one generations it is possible to have non-trivial solutions for Eq. 18 which have large mixing between light and heavy leptons, as have been shown in Refs. [15] and [16]. The cases with small and large mixing have very different experimental signatures. The small mixing solution case will lead to a visible displaced vertex in the detector at the LHC. While for the large mixing case, one can also study single heavy lepton production [16]. The aim of this paper is to study the correlations of heavy lepton productions and decays with low energy neutrino oscillation parameters and masses. Therefore in this section we will discuss constraints on the physical parameters for small mixing solutions.

A. Neutrino Masses, Mixing and the Coupling Matrix V_{lN}

On the right-handed side of Eq. 18, the parameters involved are in principle measurable parameters, the neutrino masses and mixing angles. Therefore in order to understand the constraints we need to know as much as these parameters. As has been mentioned before that in our case the V_{PMNS} is, in general, not unitary. However, since the deviation is of order $Y_\Sigma v / M_\Sigma$, to a good approximation, we can neglect these

corrections and use a unitary matrix to represent it which can be written as

$$V_{PMNS} = \begin{pmatrix} c_{12}c_{13} & c_{13}s_{12} & e^{-i\delta}s_{13} \\ -c_{12}s_{13}s_{23}e^{i\delta} - c_{23}s_{12} & c_{12}c_{23} - e^{i\delta}s_{12}s_{13}s_{23} & c_{13}s_{23} \\ s_{12}s_{23} - e^{i\delta}c_{12}c_{23}s_{13} & -c_{23}s_{12}s_{13}e^{i\delta} - c_{12}s_{23} & c_{13}c_{23} \end{pmatrix} \times \text{diag}(e^{i\Phi_1/2}, 1, e^{i\Phi_2/2}), \quad (19)$$

where $s_{ij} = \sin \theta_{ij}$, $c_{ij} = \cos \theta_{ij}$, $0 \leq \theta_{ij} \leq \pi/2$ and $0 \leq \delta \leq 2\pi$. The phase δ is the Dirac CP phase, and Φ_i are the Majorana phases. The experimental constraints on the neutrino masses and mixing parameters, at 2σ level [23], are

$$\begin{aligned} 7.25 \times 10^{-5} \text{ eV}^2 < \Delta m_{21}^2 < 8.11 \times 10^{-5} \text{ eV}^2, \quad 2.18 \times 10^{-3} \text{ eV}^2 < |\Delta m_{31}^2| < 2.64 \times 10^{-3} \text{ eV}^2, \\ 0.27 < \sin^2 \theta_{12} < 0.35, \quad 0.39 < \sin^2 \theta_{23} < 0.63, \quad \sin^2 \theta_{13} < 0.040, \end{aligned} \quad (20)$$

and no constraints on the phases. The neutrino masses are bounded by $\sum_i m_i < 1.2 \text{ eV}$ [24].

For a complete discussion of these constraints see reference [4]. Following the convention, we denote the case $\Delta m_{31}^2 > 0$ as the normal hierarchy (NH) and otherwise the inverted hierarchy (IH). In our later discussions unless specified for the input values of relevant parameters, when scanning the parameters space we will always allow $s_{12,13,23}$ to run the above allowed ranges, and the lightest neutrino mass for NH and IH cases to run the range $10^{-4} \sim 0.4 \text{ eV}$.

Eq. 18 relates V_{LN} to low energy measurable quantities, but the elements in V_{LN} can not be fully determined. Certain assumptions or new parameters need to be introduced to describe the ranges for the elements in V_{LN} . In the following we consider in details for the size of V_{LN} with the Majorana phases set to zero first, and then comment on the effects of non-zero Majorana phases.

1. Case I: Degenerate Heavy Triplet Leptons

We start with a simple but interesting case where the heavy triplet leptons are degenerate. In this case Eq. 18 becomes simple on the left hand side with $V_{LN}^* M_N^{diag} V_{LN}^\dagger = M_N \sum_{j=1,2,3} V_{LN}^{ij*2}$. Here the superscript “ i ” runs over the three light generation leptons and “ j ” runs over the three heavy triplet leptons. $M_N = M_1 = M_2 = M_3$ is the heavy triplet mass. We have a simple expression from Eq. 18

$$M_N \sum_{j=1,2,3} (iV_{LN}^{ij*})^2 = (V_{PMNS}^* m_\nu^{diag} V_{PMNS}^\dagger)_{ii} \equiv M_\nu^{ii}, \quad i = e, \mu, \tau \quad (21)$$

where $M_\nu = V_{PMNS}^* m_\nu^{diag} V_{PMNS}^\dagger$.

Explicitly we have

$$\begin{aligned}
M_N \sum_j (iV_{lN}^{ej*})^2 &= c_{13}^2 s_{12}^2 m_2 + c_{12}^2 c_{13}^2 e^{-i\Phi_1} m_1 + s_{13}^2 e^{i(2\delta-\Phi_2)} m_3, \\
M_N \sum_j (iV_{lN}^{\mu j*})^2 &= (c_{12}c_{23} - s_{12}s_{13}s_{23}e^{-i\delta})^2 m_2 + (c_{23}s_{12} + c_{12}s_{13}s_{23}e^{-i\delta})^2 e^{-i\Phi_1} m_1 \\
&\quad + c_{13}^2 s_{23}^2 e^{-i\Phi_2} m_3, \\
M_N \sum_j (iV_{lN}^{\tau j*})^2 &= (c_{12}s_{23} + c_{23}s_{12}s_{13}e^{-i\delta})^2 m_2 + (s_{12}s_{23} - c_{12}c_{23}s_{13}e^{-i\delta})^2 e^{-i\Phi_1} m_1 \\
&\quad + c_{13}^2 c_{23}^2 e^{-i\Phi_2} m_3.
\end{aligned} \tag{22}$$

If the phases in V_{lN} are all zero, the right-handed sides in the above equations are all real. We can formally write

$$M_N \sum_{j=1,2,3} (V_{lN}^{ij*})^2 = M_N \sum_{j=1,2,3} |V_{lN}^{ij}|^2. \tag{23}$$

Later when we will refer this particular case as Case I.

If indeed the three heavy triplet leptons are degenerate or almost degenerate, experimentally when they are produced, one would not be able to distinguish them and therefore must sum over the heavy ones. The above equation allows one to fix the couplings completely in terms of low energy parameters. We emphasize that this is true only for the case that all phases in V_{lN} are zero.

The experimental information on neutrino masses and mixing indicates that the neutrino mass matrix M_ν presents the following patterns

$$\begin{aligned}
M_\nu^{ee} &\ll M_\nu^{\mu\mu}, M_\nu^{\tau\tau} \quad \text{for NH}, \\
M_\nu^{ee} &> M_\nu^{\mu\mu}, M_\nu^{\tau\tau} \quad \text{for IH}.
\end{aligned} \tag{24}$$

More detailed discussions can be found in Ref. [10]. We plot the allowed values for the normalized couplings, $\sum_j |V_{lN}^{ij}|^2 M_N / 100 \text{ GeV}$, of each lepton flavor for this case in Fig. 1, as a function of the lightest neutrino mass for both the NH (left panels) and the IH (right panels) cases. We see two distinctive regions in terms of the lightest neutrino mass. In the case $m_{1(3)} < 10^{-2} \text{ eV}$, $\sum_j |V_{lN}^{ej}|^2 \ll \sum_j |V_{lN}^{\mu j}|^2, \sum_j |V_{lN}^{\tau j}|^2$ for NH and $\sum_j |V_{lN}^{ej}|^2 > \sum_j |V_{lN}^{\mu j}|^2, \sum_j |V_{lN}^{\tau j}|^2$ for IH. On the other hand, for $m_{1(3)} > 10^{-2} \text{ eV}$, we have the quasi-degenerate spectrum $\sum_j |V_{lN}^{ej}|^2 \approx \sum_j |V_{lN}^{\mu j}|^2 \approx \sum_j |V_{lN}^{\tau j}|^2$ as expected.

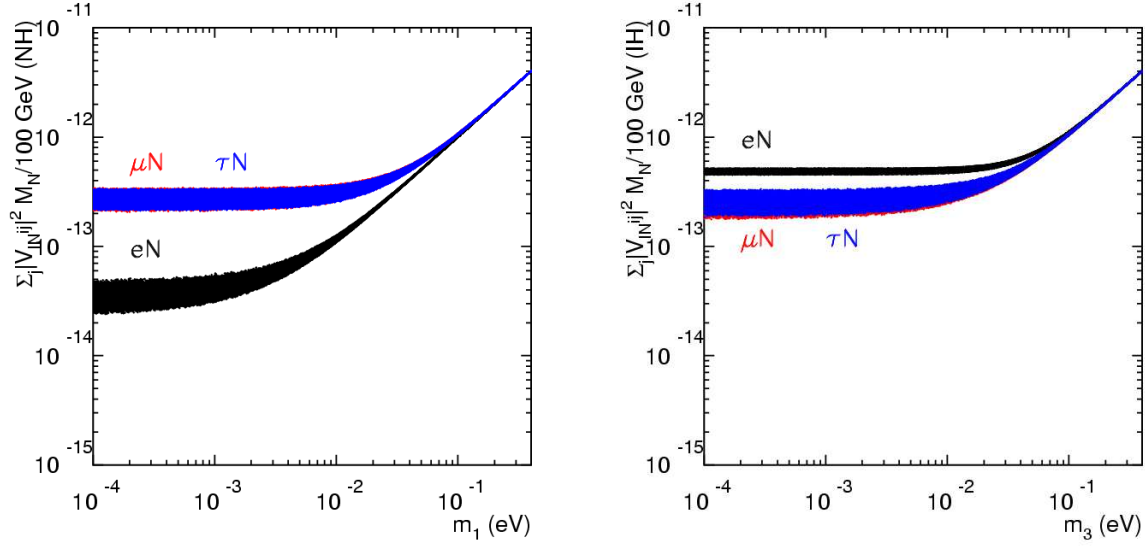


FIG. 1: $\sum_{j=1,2,3} |V_{lN}^{ij}|^2 M_N / 100 \text{ GeV}$ vs. the lightest neutrino mass for NH and IH for Case I without any phases, where areas for μ and τ flavors overlap (same for other figures).

2. Case II: A Class of Solutions for Small Mixing between Light and Heavy Neutrinos

As already mentioned before the relation in Eq.18 we can not completely fix the form for V_{lN} , but we find that V_{lN} can be written in the following form using the Casas-Ibarra parametrization [22]

$$V_{lN} = iV_{PMNS}(m_\nu^{diag})^{1/2}\Omega(w_{21}, w_{31}, w_{32})(M_N^{diag})^{-1/2}, \quad (25)$$

where $(m_\nu^{diag})^{1/2} = \text{diag}(m_1^{1/2}, m_2^{1/2}, m_3^{1/2})$, $(M_N^{diag})^{-1/2} = \text{diag}(M_1^{-1/2}, M_2^{-1/2}, M_3^{-1/2})$ and $\Omega(w_{21}, w_{31}, w_{32})$ satisfies $\Omega\Omega^T = 1$. In general the elements in Ω can be unbounded if complex variables w_{ij} are used. Since we are interested in small mixing between light and heavy neutrinos, we will limit ourselves to the case where the angles w_{ij} defined in Appendix B are real and allow them to vary in the ranges $0 < w_{21}, w_{31}, w_{32} < 2\pi$. More details about Ω are given in Appendix B where explicit expressions for V_{lN}^{ij} ($i = e, \mu, \tau, j = 1, 2, 3$) are collected.

If $\Omega = 1$, the expressions for $|V_{lN}|^2$ are simple. We have

$$\begin{aligned} M_1(|V_{lN}^{e1}|^2, |V_{lN}^{\mu1}|^2, |V_{lN}^{\tau1}|^2) &= m_1(c_{12}^2 c_{13}^2, |s_{12}c_{23} + c_{12}s_{13}s_{23}e^{i\delta}|^2, |s_{12}s_{23} - c_{12}s_{13}c_{23}e^{i\delta}|^2), \\ M_2(|V_{lN}^{e2}|^2, |V_{lN}^{\mu2}|^2, |V_{lN}^{\tau2}|^2) &= m_2(c_{13}^2 s_{12}^2, |c_{12}c_{23} - s_{12}s_{13}s_{23}e^{i\delta}|^2, |c_{12}s_{23} + s_{12}s_{13}c_{23}e^{i\delta}|^2), \\ M_3(|V_{lN}^{e3}|^2, |V_{lN}^{\mu3}|^2, |V_{lN}^{\tau3}|^2) &= m_3(s_{13}^2, c_{13}^2 s_{23}^2, c_{13}^2 c_{23}^2). \end{aligned} \quad (26)$$

Using known data on the mixing parameters, it is easy to see that $|V_{lN}^{e1}|^2 > |V_{lN}^{\mu1}|^2, |V_{lN}^{\tau1}|^2, |V_{lN}^{e2}|^2 \approx |V_{lN}^{\mu2}|^2 \approx |V_{lN}^{\tau2}|^2$, and $|V_{lN}^{\mu3}|^2, |V_{lN}^{\tau3}|^2 > |V_{lN}^{e3}|^2$ both for NH and IH cases.

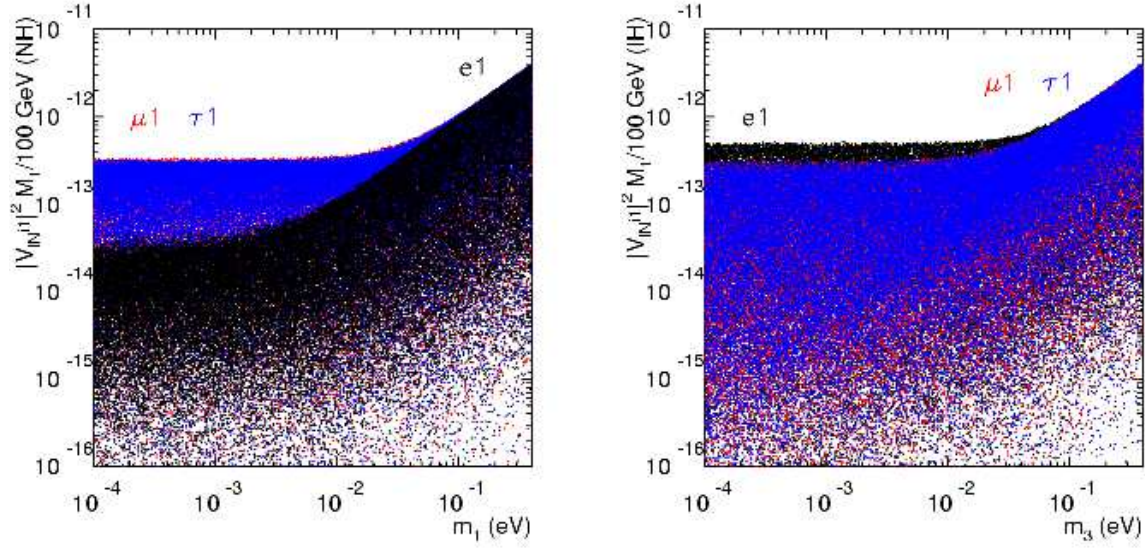


FIG. 2: $|V_{lN}^{i1}|^2 M_1 / 100 \text{ GeV}$ vs. the lightest neutrino mass for NH and IH, when $0 < w_{ij} < 2\pi$ for Case II without any phases in Ω .

To have a better understanding about the size of $|V_{lN}|^2$, we scan all w_{21} , w_{31} and w_{32} in the range $0 < w_{ij} < 2\pi$. $\Omega = 1$ case is obtained by setting $\sin(w_{ij}) = 0$. Case I discussed earlier, is also a special case of Case II.

The allowed range for the normalized coupling, $|V_{lN}^{i1}|^2 M_1 / 100 \text{ GeV}$ is shown in Fig. 2 as a function of the light neutrino mass in each spectrum. The results for the NH and IH cases are displayed in the left and right panels, respectively. The ranges of $|V_{lN}^{i2}|^2 M_2 / 100 \text{ GeV}$ and $|V_{lN}^{i3}|^2 M_3 / 100 \text{ GeV}$ are almost the same and will not be shown separately. Unlike for Case I, by just looking at the absolute values $|V_{lN}|^2$ along, it is difficult to distinguish neutrino mass hierarchies. But there are allowed regions for $|V_{lN}^{e1}|^2$ for the NH and IH which do not overlap. In this particular situation, there is still a hope to distinguish different neutrino mass hierarchies.

B. Other Constraints

In Type III seesaw model, the heavy triplet lepton masses are free parameters. The current constraint on heavy charged lepton masses comes from the direct search at collider [25], $M_E \gtrsim 100 \text{ GeV}$, which we will use as a lower bound and take $M_{E,N}$ to be larger than Higgs boson mass $M_H (> 114 \text{ GeV})$. Because the charged and neutral heavy leptons have different mass matrices, they are in general different. However the splits are small compared with the common mass term M_Σ . We will take $M_N = M_E$ as the common triplet

mass in our later discussions.

Other constraints come from electroweak precision measurements, LFV processes, and meson rare decays [6, 13, 18, 19, 25, 26], we have checked that these limits do not provide strong constraints for heavy triplet lepton decays and productions.

IV. HEAVY TRIPLET LEPTON DECAYS

In this section we study the main features of the heavy triplet lepton decays taking into account the constraints on $|V_{lN}|^2$ from the neutrino mass and mixing data as discussed in the previous section. From Eq. 18 one therefore anticipates that E and N decays could be different. We explore this in more details in the following.

A. Main Features of Heavy Triplet Lepton Decays

The partial widths for N and E decays are given by [6, 13]

$$\begin{aligned}
\Gamma(N_i \rightarrow \ell^- W^+) &= \Gamma(N_i \rightarrow \ell^+ W^-) = \frac{g^2}{64\pi} |V_{lN}^{\ell i}|^2 \frac{M_{N_i}^3}{M_W^2} \left(1 - \frac{M_W^2}{M_{N_i}^2}\right) \left(1 + \frac{M_W^2}{M_{N_i}^2} - 2\frac{M_W^4}{M_{N_i}^4}\right), \\
\sum_{m=1}^3 \Gamma(N_i \rightarrow \nu_m Z) &= \frac{g^2}{64\pi c_W^2} \sum_{\ell=e}^{\tau} |V_{lN}^{\ell i}|^2 \frac{M_{N_i}^3}{M_Z^2} \left(1 - \frac{M_Z^2}{M_{N_i}^2}\right) \left(1 + \frac{M_Z^2}{M_{N_i}^2} - 2\frac{M_Z^4}{M_{N_i}^4}\right), \\
\sum_{m=1}^3 \Gamma(N_i \rightarrow \nu_m H^0) &= \frac{g^2}{64\pi} \sum_{\ell=e}^{\tau} |V_{lN}^{\ell i}|^2 \frac{M_{N_i}^3}{M_W^2} \left(1 - \frac{M_H^2}{M_{N_i}^2}\right)^2, \\
\sum_{m=1}^3 \Gamma(E_i^+ \rightarrow \bar{\nu}_m W^+) &= \frac{g^2}{32\pi} \sum_{\ell=e}^{\tau} |V_{lN}^{\ell i}|^2 \frac{M_{E_i}^3}{M_W^2} \left(1 - \frac{M_W^2}{M_{E_i}^2}\right) \left(1 + \frac{M_W^2}{M_{E_i}^2} - 2\frac{M_W^4}{M_{E_i}^4}\right), \\
\Gamma(E_i^+ \rightarrow \ell^+ Z) &= \frac{g^2}{64\pi c_W^2} |V_{lN}^{\ell i}|^2 \frac{M_{E_i}^3}{M_Z^2} \left(1 - \frac{M_Z^2}{M_{E_i}^2}\right) \left(1 + \frac{M_Z^2}{M_{E_i}^2} - 2\frac{M_Z^4}{M_{E_i}^4}\right), \\
\Gamma(E_i^+ \rightarrow \ell^+ H^0) &= \frac{g^2}{64\pi} |V_{lN}^{\ell i}|^2 \frac{M_{E_i}^3}{M_W^2} \left(1 - \frac{M_H^2}{M_{E_i}^2}\right)^2.
\end{aligned} \tag{27}$$

In the above, we have used the relation [6]

$$\sum_{m=1}^3 |(V_{PMNS}^\dagger V_{lN})^{mi}|^2 = \sum_{\ell=e}^{\tau} |V_{lN}^{\ell i}|^2. \tag{28}$$

One can see that all E and N decay partial widths are proportional to $|V_{lN}|^2$ and the branching ratios of the cleanest channels have relationship $BR(N \rightarrow \ell^\pm W^\mp) = BR(E^\pm \rightarrow \ell^\pm Z)$ for large triplet mass. In Fig. 3 we show the branching fractions for the decays of N (left) and E (right) versus their masses with $M_{H^0} = 120$ GeV for Cases I and II, in which the lepton and neutrino flavors in final state are summed.

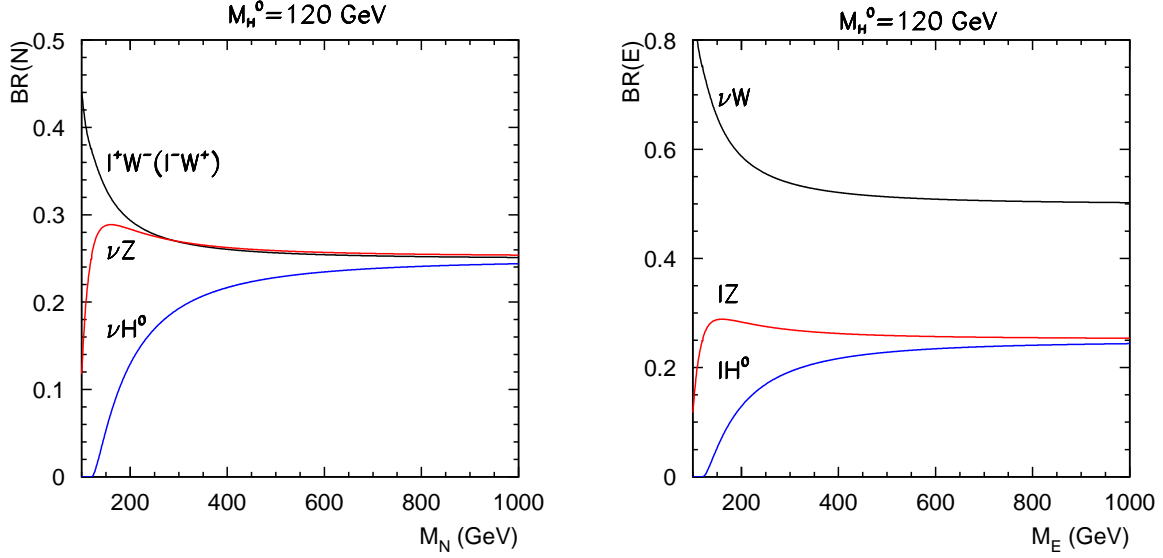


FIG. 3: Branching fractions of N and E^\pm .

Since all partial widths are proportional to $\sum_{\ell=e}^{\tau} |V_{lN}^{\ell i}|^2$, there are no other free parameters for the branching ratios displayed in the figure.

B. Heavy Triplet Lepton Decays And Neutrino Mass Spectra

We now present our results for decay branching ratios in detail for Cases I and II described before.

1. Case I

In Fig. 4 we show the impact of the neutrino masses and mixing angles on the branching fractions summing all N_i decaying into e, μ, τ lepton plus W boson respectively, with the left panels for NH and the right panels for IH. The branching fraction can differ by one order of magnitude in NH case with $BR(\mu^\pm W^\mp), BR(\tau^\pm W^\mp) \gg BR(e^\pm W^\mp)$, and about a few times of magnitude in the IH spectrum with $BR(e^\pm W^\mp) > BR(\mu^\pm W^\mp), BR(\tau^\pm W^\mp)$. As expected that all the channels are quite similar when the neutrino spectrum is quasi-degenerate, $m_1 \approx m_2 \approx m_3 \geq 0.1$ eV.

2. Case II

We show the branching fractions of processes $N_1 \rightarrow \ell^\pm W^\mp$ ($\ell = e, \mu, \tau$) as functions of the lightest neutrino mass for NH and IH, when $M_1 = 300$ GeV, in Fig. 5. The behaviors of N_2 and N_3 decays are

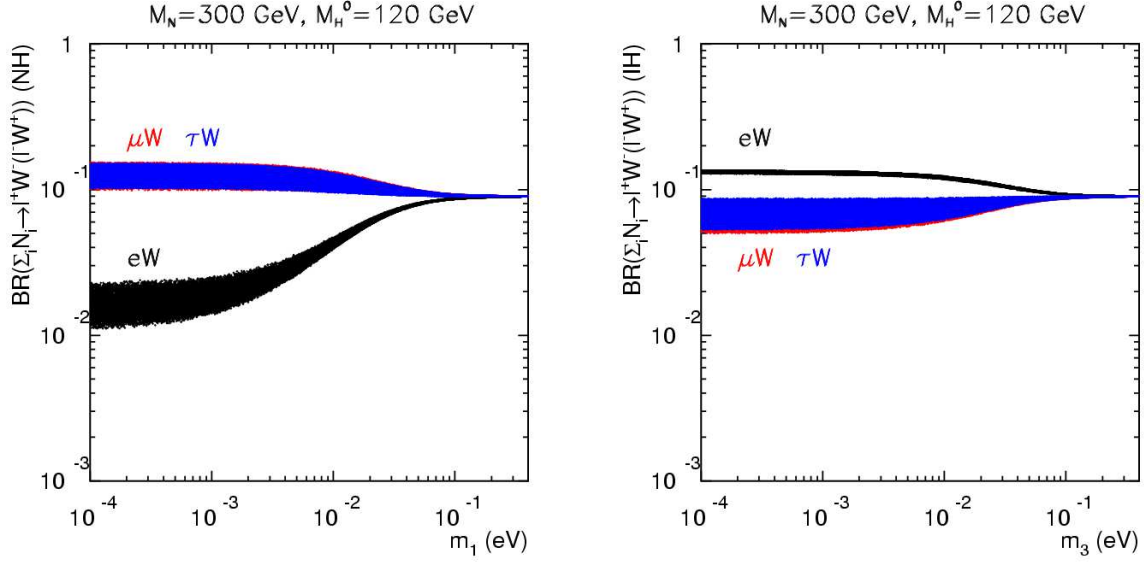


FIG. 4: The branching fractions of $\sum_{i=1,2,3} N_i \rightarrow \ell^\pm W^\mp$ ($\ell = e, \mu, \tau$) for NH and IH versus lightest neutrino mass when $M_N = 300$ GeV, $M_{H^0} = 120$ GeV for Case I without any phases.

almost the same. These do not seem to provide discrimination power between the two mass spectra.

It is important to note that nature would choose only one specific form of Ω , not a random selection. To illustrate in fact that detailed analysis can still distinguish different neutrino mass spectra in each special case, we show in Fig. 6 the branching fractions of N_1 as functions of the lightest neutrino mass for NH and IH, respectively, with $M_1 = 300$ GeV, and $w_{21} = w_{31} = 0.2\pi$. Note that N_1 decay does not depend on w_{32} . We see that the branching fractions for NH and IH cases can be substantially different, $BR(\mu^\pm W^\mp) > BR(\tau^\pm W^\mp) > BR(e^\pm W^\mp)$ in NH and $BR(e^\pm W^\mp) \gg BR(\mu^\pm W^\mp), BR(\tau^\pm W^\mp)$ in IH.

The above analysis can only be useful if there are independent ways that the angles w_{ij} and phases can be measured. We have not been able to find viable method to achieve this. We therefore would like to turn the argument around that if in the future the neutrino mass hierarchy is measured, then in combination with the possible information on the sizes of the elements in V_{LN} from our later discussions in Sec. V.C., information on the model parameters w_{ij} and phases may be extracted at the LHC.

C. Impact of Majorana Phases for E and N Decays

So far we have assumed that the Majorana phases are all zero. The unknown Majorana phases could modify the predictions for E and N decays. In this section we study the effect of non-zero Majorana phases on E and N decays. We note that in general there are two Majorana phases, $\Phi_{1,2}$, and a general analysis

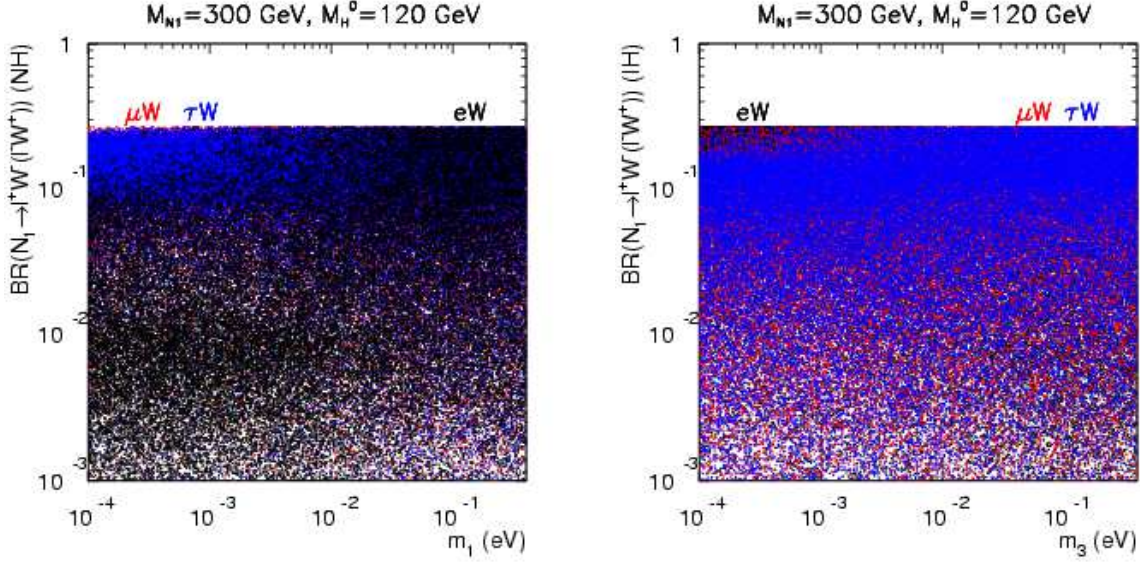


FIG. 5: Branching fractions of process $N_1 \rightarrow \ell^\pm W^\mp$, $\ell = e, \mu, \tau$ vs. the lightest neutrino mass for NH and IH, when $M_1 = 300$ GeV, $M_{H^0} = 120$ GeV and $0 < w_{ij} < 2\pi$ for Case II without any phases in Ω .

will be complicated. The situation can be simplified for some special cases. From Appendix B, it can be easily seen that in the limits that $m_1 = 0$ and $m_3 = 0$, the phase Φ_1 and Φ_2 drop off the expressions for V_{LN} , respectively. The $m_1 = 0$ can happen for normal hierarchy, and $m_3 = 0$ can happen for inverted hierarchy neutrino mass patterns. We therefore will take these two cases for illustrations. Note that with non-zero Majorana phases, it is not possible to have Case I any more. Our discussion here will only apply to Case II. The V_{LN} dependence on Majorana phases for Case II can be read off from Appendix B. The two illustration cases are:

- a. *NH with one massless neutrino* ($m_1 \approx 0$). In this case the E and N decay rates depend on only one Majorana phase Φ_2 .
- b. *IH with one massless neutrino* ($m_3 \approx 0$). In this case E and N decay rates depend on only one phase Φ_1 .

In Fig. 7 we show the dependence of N_1 decay rates with Majorana phases Φ_2 and Φ_1 in NH and IH respectively without any phases in Ω . The dependence of N_2 and N_3 decays on Majorana phases are almost the same as that of N_1 . For Φ_2 from 0 to π in NH, they are always $\mu W, \tau W$ channels that dominate. And for Φ_1 from 0 to π in IH, eW channel always dominates. To cover the whole ranges the range of Majorana phases needs to go from 0 to 4π according to our definition in Eq. 19. But for the fully scanned plot Fig. 7 the range from 0 to 2π can reflect the complete feature. The figures are symmetric from 2π to 4π to the ones from 0 to 2π . We see that the Majorana phases do have impact on the branching ratios. One can extract

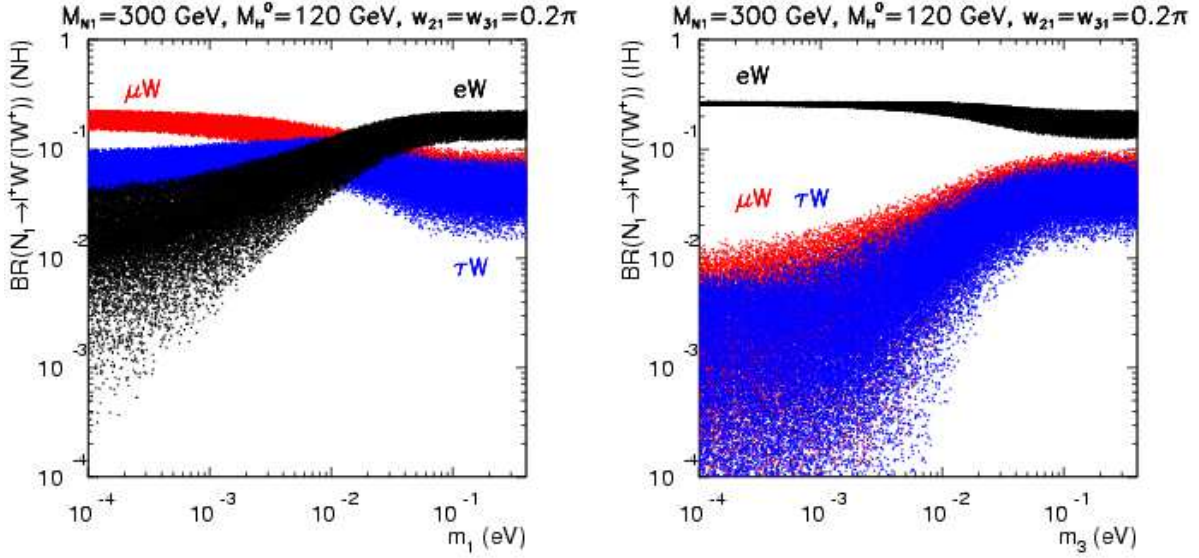


FIG. 6: Branching fractions of process $N_1 \rightarrow \ell^\pm W^\mp$, $\ell = e, \mu, \tau$ vs. the lightest neutrino mass for NH and IH, with $M_1 = 300$ GeV, and $w_{21} = w_{31} = 0.2\pi$ for Case II without any phases in Ω .

information on Majorana phase from different lepton-flavor final states. One can also study more detailed correlations of the NH and IH cases with the change of Majorana phases which we show indicative plots for the above two cases in Fig. 8. We can see that for NH when the phase $\Phi_2 = 2\pi$, one obtains the maximal suppression (enhancement) for channel $N_1 \rightarrow \mu^\pm W^\mp$ ($N_1 \rightarrow \tau^\pm W^\mp$) by one order. For IH the maximal suppression and enhancement takes place also when $\Phi_1 = 2\pi$. In this case the dominate channels swap from $N_1 \rightarrow e^\pm W^\mp$ when $\Phi_1 = 0$ to $N_1 \rightarrow \mu^\pm W^\mp, \tau^\pm W^\mp$ when $\Phi_1 = 2\pi$. This qualitative change can be of useful in extracting the value of the Majorana phase Φ_1 .

D. Total Decay Width of Heavy Triplet Leptons

To complete our study about the heavy lepton and neutrino properties, in Fig. 9 we plot the total width (left axis) and decay length (right axis) for N versus M_N in NH and IH for Case II. The total decay width is proportional to $M_\nu M_N^2$. Although not considered as long-lived for large triplet mass, the E and N decay could lead to a visible displaced vertex in the detector at the LHC. This displaced vertex can be observed through E and N reconstructions as first pointed out by Ref. [11]. Careful analysis of displaced vertex can also provide crucial information about neutrino mass hierarchy since the NH and IH cases have different decay widths as can be seen from Figs. 6, 8, and also the right panel in Fig. 9. Since we cannot separately determine each of the heavy triplet lepton decays for Case I. It is not possible to give a similar description

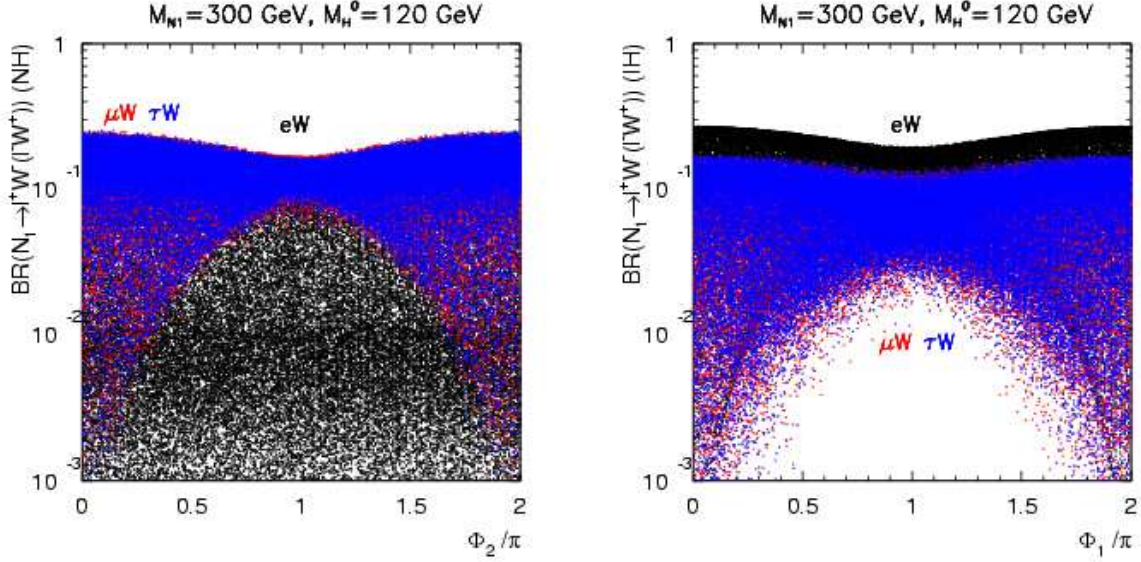


FIG. 7: The branching fractions of $N_1 \rightarrow \ell^\pm W^\mp$ versus Majorana phase Φ_2 for NH and Φ_1 for IH with $M_1 = 300$ GeV, $M_{H^0} = 120$ GeV and $0 < w_{ij} < 2\pi$ for Case II without any phases in Ω .

about the decay length. But this case is just a special case of Case II which are already implicitly included in the results for Case II.

V. HEAVY TRIPLET LEPTON PRODUCTIONS AT THE LHC

In this section we study the main production mechanisms of heavy triplet leptons and their experimental signatures at the LHC. There are existing previous literatures on this topic, both in theoretical and phenomenological considerations [11, 13, 25]. The main production channels of E^\pm, N are

$$pp \rightarrow \gamma^*/Z^* \rightarrow E^+ E^-, \quad pp \rightarrow W^* \rightarrow E^\pm N. \quad (29)$$

The relevant total production cross sections are plotted in Fig. 10. Note that the production cross sections for $E^+ N$ and $E^- N$ are different due to the fact that the LHC is a pp machine.

We can see that up to 1.5 TeV, the cross section for each production mode is a few times larger than $0.01 fb$. It gives the hope that with enough integrated luminosity, saying $300 fb^{-1}$, LHC may be able to probe the scale up to 1.5 TeV if all three production modes are analyzed. However, one should be more careful in carrying out the analysis beyond the naive total cross section estimate. One has to make appropriate cuts to reduce SM backgrounds which will also reduce the signal rate.

The detection of E^\pm and N are through their decays into SM particles. We have studied the main decay

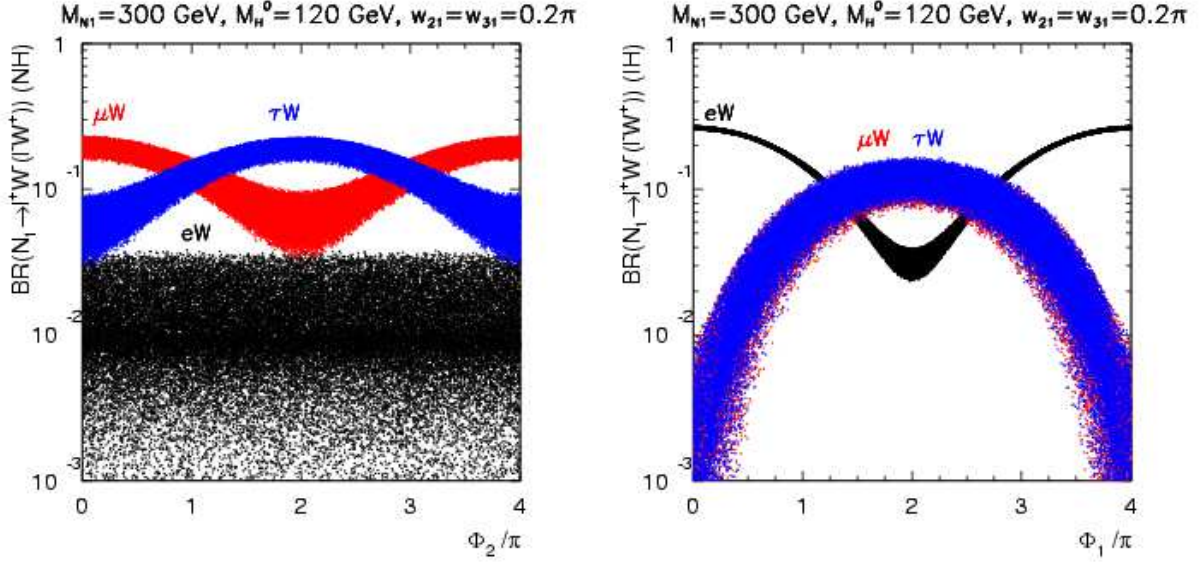


FIG. 8: The branching fractions of $N_1 \rightarrow \ell^\pm W^\mp$ versus Majorana phase Φ_2 for NH and Φ_1 for IH with $M_1 = 300$ GeV, $M_{H^0} = 120$ GeV, and $w_{21} = w_{31} = 0.2\pi$ for Case II without any phases in Ω .

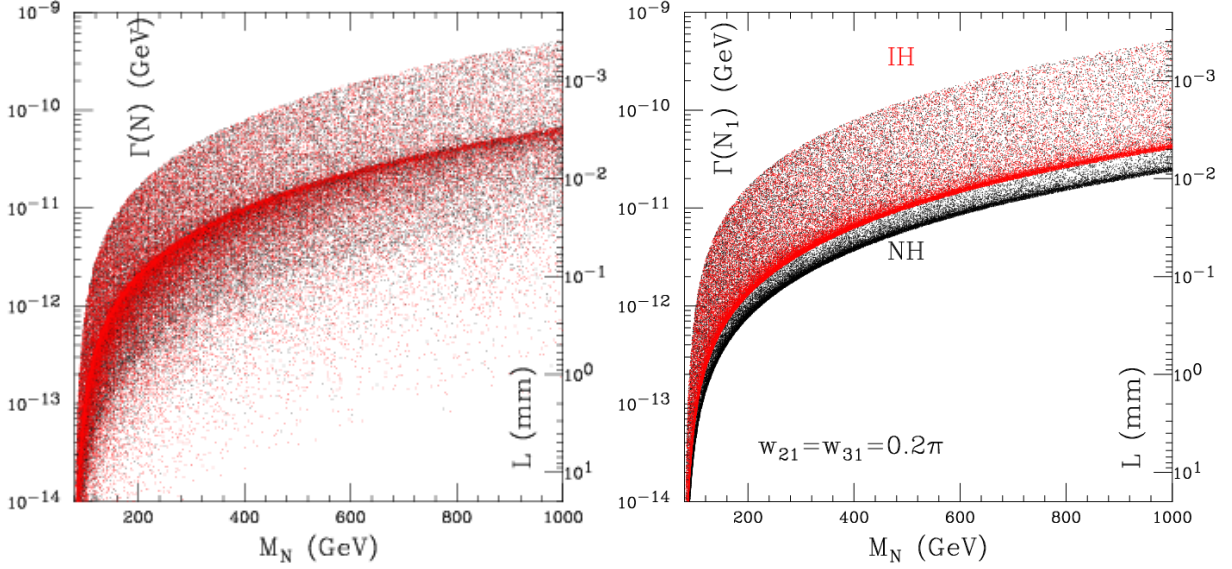


FIG. 9: The left and right panels are for the total decay widths of N_1 with $M_{H^0} = 120$ GeV for w_{ij} scanned in their whole allowed ranges, and for $w_{21} = w_{31} = 0.2\pi$, respectively.

modes, $E^\pm \rightarrow \ell^\pm Z, \nu W^\pm, \ell^\pm H^0$ and $N \rightarrow \ell^\pm W^\mp, \nu Z, \nu H^0$ in previous sections. The signal channels for E^\pm and N productions can be classified according to charged usual leptons in the final states [13]: i) 6 charged leptons $\ell^\pm \ell^\pm \ell^\pm \ell^\mp \ell^\mp \ell^\mp$; ii) 5 charged leptons $\ell^\pm \ell^\pm \ell^\mp \ell^\mp \ell^\pm$; iii) 4 charged leptons $\ell^\pm \ell^\pm \ell^\pm \ell^\mp$; iv) 4 charged leptons $\ell^+ \ell^+ \ell^- \ell^-$; v) 3 charged leptons $\ell^\pm \ell^\pm \ell^\mp$; vi) 2 charged leptons $\ell^\pm \ell^\pm$; vii) 2 charged

leptons $\ell^+\ell^-jjjj$; And viii) 1 charged lepton $\ell^\pm jjjj$.

With the heavy triplet leptons fixed at a mass of 300 GeV, it has been shown that signals from i) and ii) have too small cross sections. They are not good for discovery. Signals from iii) and iv) can provide clean measurement of the heavy triplet masses. Signals from v) and vi) have excellent potential for the discovery with relatively high signal rate and small background. Signals from vii) and viii) have large cross sections, but large background [13]. We will not carry out a full comprehensive study of all possible final states, but concentrate on two types of particular final states, belonging to iv) and vi), which represent two ideal signals for E^+E^- and $E^\pm N$ productions.

These two types of signals are: 1) $pp \rightarrow E^+E^- \rightarrow \ell^+Z(\rightarrow \ell^+\ell^-)\ell^-Z(\rightarrow qq)$, and 2) $pp \rightarrow E^\pm N \rightarrow \ell^\pm Z(\rightarrow q\bar{q})\ell^\pm W^\mp(\rightarrow q\bar{q}')$. We note that all the particles in the final states in these two processes can be measured and the masses of E and N can, in principle, be reconstructed. Therefore these processes are easier to control compared with those with multi-neutrinos in the final states. Replacing Z by H^0 can also result in the same final states. Since Higgs boson mass is not known yet, we will not consider them. This type of events can be eliminated with reconstruction of Z mass.

Our approach beyond the existing studies is to make concrete predictions of the E^\pm and N signals in connection with the neutrino oscillation parameters through Eq. 18, and allow the heavy triplet lepton masses to vary. We also include τ events reconstruction which turns out to provide some interesting information.

We now discuss the observability at the LHC in detail. In sub-sec. A and B, we are mainly concerned with the kinematical features for the signal and backgrounds. We will take the decay branching fractions of E and N to be 100% to the corresponding channels under discussions. In sub-sec. C, we will devote ourselves to the determination for the branching fractions. We also assume that the three heavy triplet leptons are hierarchical and consider the lightest one of them. We will comment on degenerate case as described in Case I previously at the end.

A. E^+E^- pair production

In this case, one of the cleanest ways to make sure signals are from E^+E^- production is to use the decay mode

$$E^\pm \rightarrow \ell^\pm Z \quad (\ell = e, \mu, \tau) \quad (30)$$

and analyze

$$E^+E^- \rightarrow \ell^+Z(\rightarrow \ell^+\ell^-)\ell^-Z(\rightarrow q\bar{q}). \quad (31)$$

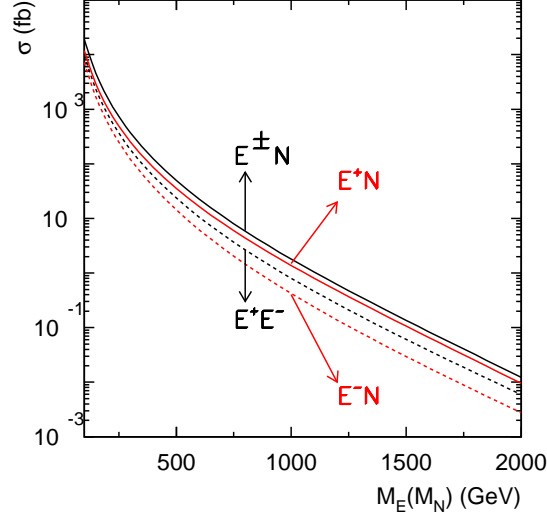


FIG. 10: Heavy lepton production total cross section at the LHC versus its mass. The black dashed curve is for $pp \rightarrow E^+ E^-$. The black solid curve is for $pp \rightarrow E^\pm N$ via W^\pm exchange, assuming $M_E = M_N$. The two red curves are for $pp \rightarrow E^+ N$ (solid) and $pp \rightarrow E^- N$ (dashed) respectively.

We will explore the signal observability according to the different lepton flavors.

$$1. \quad E^+ E^- \rightarrow \ell^+ \ell^+ \ell^- \ell^- jj \quad (\ell = e, \mu)$$

For this case, the leading irreducible SM backgrounds to this channel are

$$\begin{aligned} \ell^+ \ell^- Z(\rightarrow \ell^+ \ell^-) jj &\rightarrow \ell^+ \ell^+ \ell^- \ell^- jj, \\ t(\rightarrow b W^+(\rightarrow \ell^+ \nu)) \bar{t}(\rightarrow \bar{b} W^-(\rightarrow \ell^- \bar{\nu})) Z(\rightarrow \ell^+ \ell^-) &\rightarrow \ell^+ \ell^+ \ell^- \ell^- jj + \cancel{E}_T. \end{aligned} \quad (32)$$

We generate the SM backgrounds using MadGraph.

Although the background rates are very large to begin with, the kinematics is quite different between the signal and the backgrounds. We employ the following basic acceptance cuts for the event selection [27]

$$\begin{aligned} p_T(\ell) &\geq 15 \text{ GeV}, \quad |\eta(\ell)| < 2.5, \\ p_T(j) &\geq 25 \text{ GeV}, \quad |\eta(j)| < 3.0, \\ \Delta R_{jj}, \Delta R_{j\ell}, \Delta R_{\ell\ell} &\geq 0.4. \end{aligned} \quad (33)$$

where p_T is the transverse momentum, η is the pseudo-rapidity and ΔR is the separation between events for any of the pairs ℓ and ℓ , ℓ and j , and, j and j .

To simulate the detector effects on the energy-momentum measurements, we smear the electromagnetic energy and jet energy by a Gaussian distribution whose width is parameterized as [27]

$$\begin{aligned}\frac{\Delta E}{E} &= \frac{a_{cal}}{\sqrt{E/\text{GeV}}} \oplus b_{cal}, \quad a_{cal} = 10\%, \quad b_{cal} = 0.7\%, \\ \frac{\Delta E}{E} &= \frac{a_{had}}{\sqrt{E/\text{GeV}}} \oplus b_{had}, \quad a_{had} = 50\%, \quad b_{had} = 3\%.\end{aligned}\quad (34)$$

With further judicious cuts, the background can be reduced more. We outline the characteristics and propose some judicious cuts as follows.

- For a few hundred GeV E , the leptons from heavy triplet lepton decays are very energetic. We therefore tight up the kinematical cuts with

$$p_T^{max}(\ell) > M_E/4, \quad p_T^{max}(j) > 50 \text{ GeV}. \quad (35)$$

- To reconstruct Z boson, we select among four possibilities of opposite sign lepton pair $\ell^+\ell^-$ and take advantage of the feature $M_{\ell_1^+\ell_2^-} = M_{jj}$. In practice, we take their invariant masses close to M_Z with $|M_{\ell_1^+\ell_2^-,jj} - M_Z| < 15 \text{ GeV}$.
- To reconstruct heavy lepton E , we take advantage of the feature that two E 's have equal mass $M_{\ell_1^+\ell_2^-\ell_3^\pm} = M_{jj\ell_4^\mp}$. In practice, we take $|M_{\ell_1^+\ell_2^-\ell_3^\pm} - M_{jj\ell_4^\mp}| < M_E/25$. This helps for the background reduction, in particular for $\ell^+\ell^-Zjj$.
- To remove the $t\bar{t}Z$ background, we veto the events with large missing energy from W decay $\cancel{E}_T < 20 \text{ GeV}$.

The production cross section of E^+E^- signal with basic cuts (solid curve) and all of the cuts (dotted curve) above are plotted in Fig. 11. For comparison, the background processes of $\ell^+\ell^-Zjj$ and $t\bar{t}Z$ are also included with the sequential cuts as indicated. The backgrounds are suppressed substantially.

Finally, when we perform the signal significance analysis, we look for the resonance in the mass distribution of $\ell_1^+\ell_2^-\ell_3^\pm$ and $jj\ell_4^\mp$. The invariant masses of them are plotted in Fig. 12 for 300 GeV E pair production. If we look at a mass window of $|M_{\ell_1^+\ell_2^-\ell_3^\pm,jj\ell_4^\mp} - M_E| < M_E/20$, the backgrounds will be at a negligible level.

As a remark, we would like to comment on the other potentially large, but reducible backgrounds, like $t\bar{t}jj$. The $t\bar{t}jj$ production rate is very high, leading to the $\ell^+\ell^-X$ final state with about 40 pb. Demanding another isolated lepton presumably from the b quarks and with the basic cuts, the background rate will be reduced by about three to four orders of magnitude. The stringent lepton isolation cut for multiple charged leptons can substantially remove the b -quark cascade decays. With the additional $M_{jj}, M_{\ell^+\ell^-}, M_{\ell^+\ell^-\ell^\pm}, M_{jj\ell^\mp}$ cuts, the backgrounds should be under control.

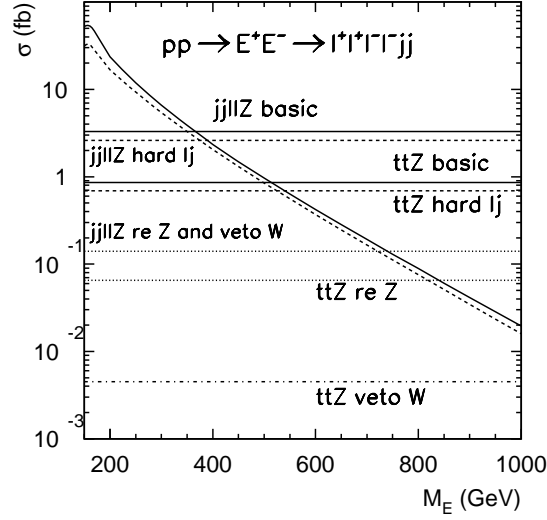


FIG. 11: Production cross section of E^+E^- with basic cuts (solid) and hard final states cuts (dashed). Branching fractions for E decay are not included in this plot. For comparison, the background processes are also included with the sequential cuts as indicated.

$$2. \quad E^+E^- \rightarrow \tau^\pm \ell^\mp \ell^+ \ell^- jj, \tau^+ \tau^- \ell^+ \ell^- jj$$

The τ lepton final state from E decay can provide additional information. Its identification and reconstruction are different from e, μ final states because a τ decays promptly and there will always be missing neutrinos in τ decay products.

In order to reconstruct the events with τ 's we note that all the τ 's are very energetic from the decay of a few hundred GeV heavy lepton E . The missing momentum will be along the direction of the charged track. We thus assume the momentum of the missing neutrinos to be reconstructed by

$$\vec{p}(\text{invisible}) = \kappa \vec{p}(\text{track}). \quad (36)$$

Identifying $\vec{p}_T(\text{invisible})$ with the measured \cancel{E}_T , we thus obtain the τ momentum by

$$\vec{p}_T(\tau) = \vec{p}_T(\ell) + \cancel{E}_T, \quad p_L(\tau) = p_L(\ell) + \frac{\cancel{E}_T}{p_T(\ell)} p_L(\ell).$$

The E pair kinematics is, thus, fully reconstructed. The reconstructed invariant masses of $M(\ell_1^+ \ell_2^- \tau^\pm)$ and $M(jj \ell^\mp)$ are plotted in Fig. 13. We see that $M(\ell_1^+ \ell_2^- \tau^\pm)$ distribution (solid curve) is slightly broader as anticipated. We always can find the rather narrow mass distribution. The $jj \ell^\mp$ system right here (dashed curve) serves as the most distinctive kinematical feature for the signal identification. Of course the single τ

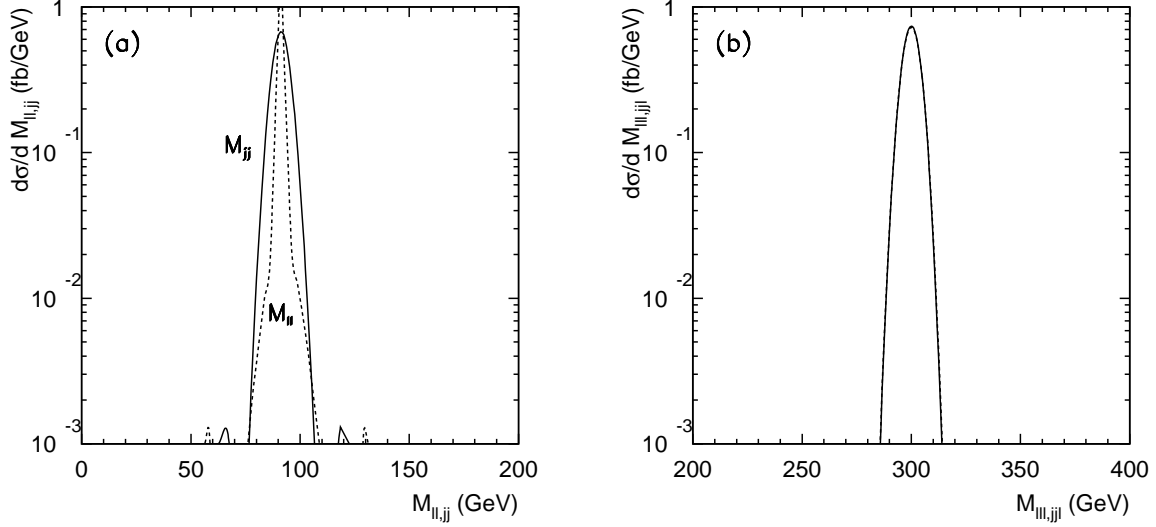


FIG. 12: Reconstructed invariant mass of $M(\ell_1^+\ell_2^-), M(jj)$ (a) and $M(\ell_1^+\ell_2^-\ell_3^\pm), M(jj\ell_4^\pm)$ (b) for $\ell^+\ell^+\ell^-\ell^-jj$ production, with a E mass of 300 GeV.

lepton could also be produced with the hadronic decay Z boson from the same parent E . The feature in this case is the same.

For $\tau^+\tau^-\ell^+\ell^-jj$ events with two τ 's, we generalize the momenta reconstruction to

$$\vec{p}(\text{invisible}) = \kappa_1 \vec{p}(\text{track}_1) + \kappa_2 \vec{p}(\text{track}_2). \quad (37)$$

The proportionality constants κ_1 and κ_2 can be determined from the missing energy measurement as long as the two charge tracks are linearly independent. In practice when we wish to identify the events with τ 's, we require a minimal missing transverse energy

$$\cancel{E}_T > 20 \text{ GeV}. \quad (38)$$

This will effectively separate them from the $\ell^+\ell^+\ell^-\ell^-jj$ events.

Another important difference between the leptons from the primary E decay and from the τ decay is that the latter is much softer. In Fig. 14 we show the p_T distribution of the softer lepton from the heavy lepton and τ decays in the events of $\ell^+\ell^+\ell^-\ell^-jj$, $\tau^\pm\ell^\mp\ell^+\ell^-jj$ and $\tau^+\tau^-\ell^+\ell^-jj$.

Note that the two τ 's could be produced from either two heavy leptons or Z boson. It is easy to distinguish the two cases. Firstly it is the two hard e, μ leptons that reconstruct Z boson when two τ 's are from E decay, but if two τ 's reconstruct Z boson the invariant mass distribution must be much broader. We plot the reconstructed invariant mass distributions of $M(\ell^+\ell^-)$ and $M(\tau^+\tau^-)$ in Fig. 15. On the other hand,

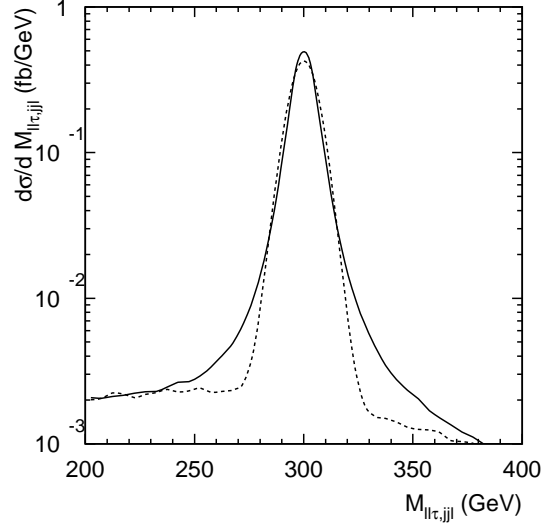


FIG. 13: Reconstructed invariant mass of $M(\ell_1^+ \ell_2^- \tau^\pm)$ (solid), $M(jj\ell^\pm)$ (dashed) for $\tau^\pm \ell^\mp \ell^- \ell^- jj$ production, with a E mass of 300 GeV.

for E reconstruction, the invariant masses of $\tau^\pm \ell^+ \ell^-$ and $\tau^\mp jj$ are almost the same. But that of $\ell^\pm \tau^+ \tau^-$ is broader than $\ell^\mp jj$, see Fig. 16.

B. $E^\pm N$ associated production

In this case the cleanest decay modes of E^\pm and N are

$$E^\pm \rightarrow \ell^\pm Z, \quad N \rightarrow \ell^\pm W^\mp \quad (\ell = e, \mu, \tau) \quad (39)$$

and the signals for $E^\pm N$ associated production are

$$E^\pm N \rightarrow \ell^\pm Z (\rightarrow q\bar{q}) \ell^\pm W^\mp (\rightarrow q\bar{q}'). \quad (40)$$

We employ the same basic acceptance cuts and smearing parameters as in the previous section. The leading irreducible SM background to this channel is

$$t\bar{t}W^\pm \rightarrow \ell^\pm \ell^\pm jjjj + \cancel{E}_T. \quad (41)$$

The QCD processes $jjjjW^\pm W^\pm, jjW^\pm W^\pm W^\mp$ are much smaller. This is estimated based on the fact that QCD induced $jjW^\pm W^\pm \rightarrow jj\ell^\pm \ell^\pm \cancel{E}_T$ is about 15 fb. With an additional α_s^2 and 6 body phase space or one more W suppression, they are much smaller than $t\bar{t}W^\pm$. Other EW backgrounds $WWWW, WWWZ$ are also negligible.

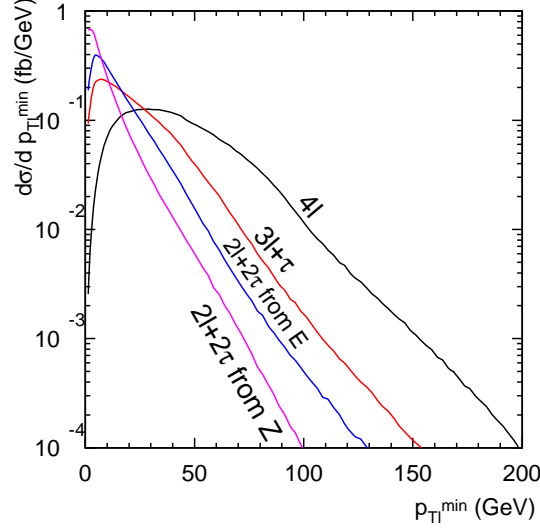


FIG. 14: p_T distribution of the softer lepton from the heavy lepton E and τ decays in the events of $\ell^+\ell^+\ell^-\ell^-jj$, $\tau^\pm\ell^\mp\ell^+\ell^-jj$ and $\tau^+\tau^-\ell^+\ell^-jj$, for a E mass of 300 GeV.

We again apply further judicious cuts as following to reduce the background,

- We set additional cuts for hard leptons and jets

$$p_T^{max}(\ell) > M_E/4, \quad p_T^{max}(j) > 50 \text{ GeV}. \quad (42)$$

- To reconstruct Z and W boson masses, we select two pair jets among the four ones and take their invariant masses closest to M_Z and M_W with $|M_{j_1j_2} - M_Z(M_{j_3j_4} - M_W)| < 15 \text{ GeV}$. Their invariant masses are plotted in Fig. 17 (a).
- To reconstruct heavy lepton E and N , we take advantage of the feature that they have equal mass $M_{\ell_1j_1j_2} = M_{\ell_2j_3j_4}$. In practice, we take $|M_{\ell_1j_1j_2} - M_{\ell_2j_3j_4}| < M_E/25$. This helps for the background reduction.
- To remove the $t\bar{t}Z$ background, we veto the events with large missing energy from W decay $\cancel{E}_T < 20 \text{ GeV}$.

Next, when we perform the signal significance analysis, we look for the resonance in the mass distribution of $\ell_1j_1j_2$ and $\ell_2j_3j_4$. The invariant masses of them are plotted in Fig. 17 (b) for 300 GeV E pair production. If we look at a mass window of $|M_{\ell_1j_1j_2, \ell_2j_3j_4} - M_E| < M_E/20$, the backgrounds will be at a negligible level. The production cross section of $E^\pm N$ signal with basic cuts (solid curve) and all of the cuts (dotted

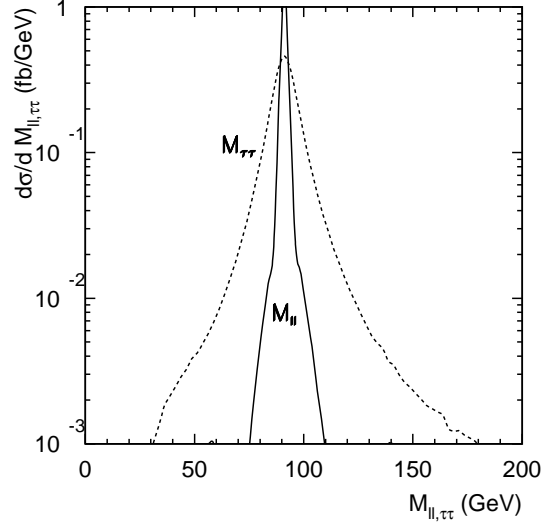


FIG. 15: Reconstructed invariant mass of $M(\ell^+\ell^-)$, $M(\tau^+\tau^-)$ for $\tau^+\tau^-\ell^+\ell^-jj$ production, with a E mass of 300 GeV.

curve) above are plotted in Fig. 18. For comparison, the background processes of $t\bar{t}W^\pm$ is also included with the sequential cuts as indicated.

Finally, we would like to give a comment for another excellent signal for $E^\pm N$ production

$$E^\pm N \rightarrow \ell^\pm Z(\rightarrow \ell^+\ell^-)\ell^\pm W^\mp(\rightarrow q\bar{q}') \quad (43)$$

This signal has almost no standard model background. However, its production rate is about 10 times lower than that we consider above. We will not study it here further.

C. Measuring Branching Fractions

So far, we have only studied the characteristic features of the signal and backgrounds for the leading channels with the decay branching fractions of E and N to be 100%. For illustration, we consider first the cleanest channel, $E^+E^- \rightarrow \mu^+Z\mu^-Z$. The number of events is written as

$$N = L \times \sigma(pp \rightarrow E^+E^-) \times \text{BR}^2(E^+ \rightarrow \mu^+Z), \quad (44)$$

where L is the integrated luminosity. Given a sufficient number of events N , the mass of E is determined by the invariant mass of three leptons and one lepton and two jets. We thus predict the corresponding production rate $\sigma(pp \rightarrow E^+E^-)$ for this given mass. The only unknown in the Eq. 44 is the decay branching

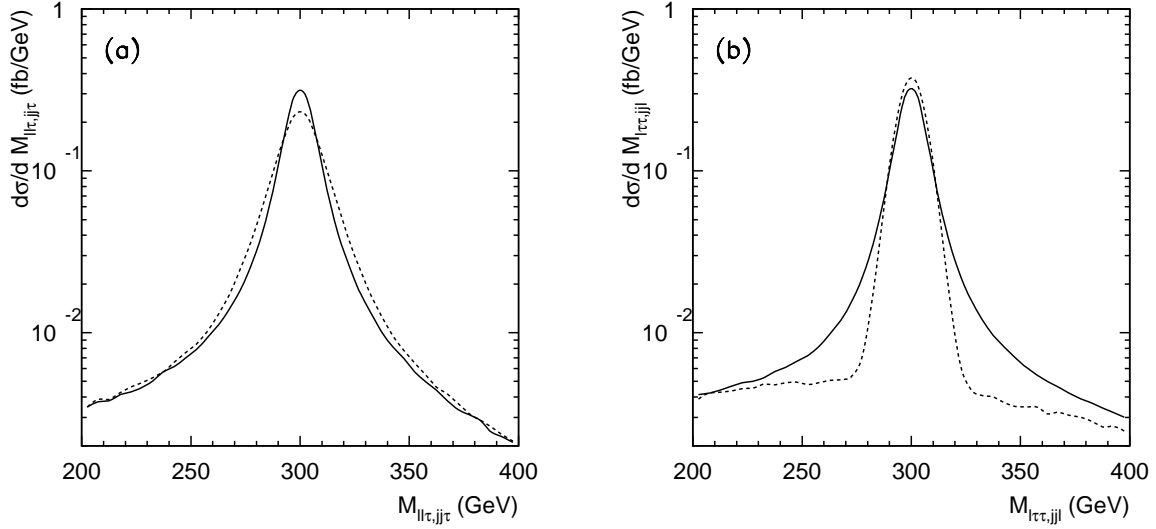


FIG. 16: Reconstructed invariant mass of $M(\tau^\pm \ell^+ \ell^-)$ (solid), $M(\tau^\pm jj)$ (dashed) (a) and $M(\ell^\pm \tau^+ \tau^-)$ (solid), $M(\ell^\pm jj)$ (dashed) (b) for $\tau^+ \tau^- \ell^+ \ell^- jj$ production, with a E mass of 300 GeV.

fraction. We present the event contours in the $BR-M_E$ plane in Figs. 19 (a) and (b) for 100 fb^{-1} and 300 fb^{-1} luminosities including all the judicious cuts described earlier, with which the backgrounds are insignificant. We see that with the estimated branching fraction for $\mu + Z$, one can reach the coverage of about $M_E \lesssim 0.8 \text{ TeV}$ for 100 fb^{-1} luminosity and $M_E \lesssim 0.9 \text{ TeV}$ for 300 fb^{-1} luminosity.

The associated $E^\pm N$ production has larger cross section compared with $E^+ E^-$ production and can provide even better signals. In Figs. 20 (a) and (b), we show the event contours in the $BR-M_E$ plane, for 100 fb^{-1} and 300 fb^{-1} luminosities including all the judicious cuts described earlier. Note again the events number for $E^+ N$ and $E^- N$ cases are different due to the LHC being a pp machine. In Fig. 21 (a) and (b) we show the event contour for $E^+ N$ and $E^- N$ separately. One can see that the LHC has tremendous sensitivity to probe the channel $E^\pm \rightarrow \mu^\pm Z$ or $N \rightarrow \mu^\pm W^\mp$ in this production mechanism. One can reach the coverage of about $M_E \lesssim 1 \text{ TeV}$ for 100 fb^{-1} luminosity and $M_E \lesssim 1.2 \text{ TeV}$ for 300 fb^{-1} luminosity.

We comment that for Case I, where the three heavy triplet charged and neutral leptons are degenerate, one can not distinguish among the three heavy particles and the detection signals will add up. This will enhance the event number by roughly a factor of 3.

As discussed earlier that in Case I, the E and N decay branching fractions and the light neutrino mass matrix are directly correlated, therefore measuring the BR's of different flavor combinations becomes crucial in understanding the neutrino mass hierarchy pattern and thus the mass generation mechanism. We find the following for Case I when all phases are neglected,

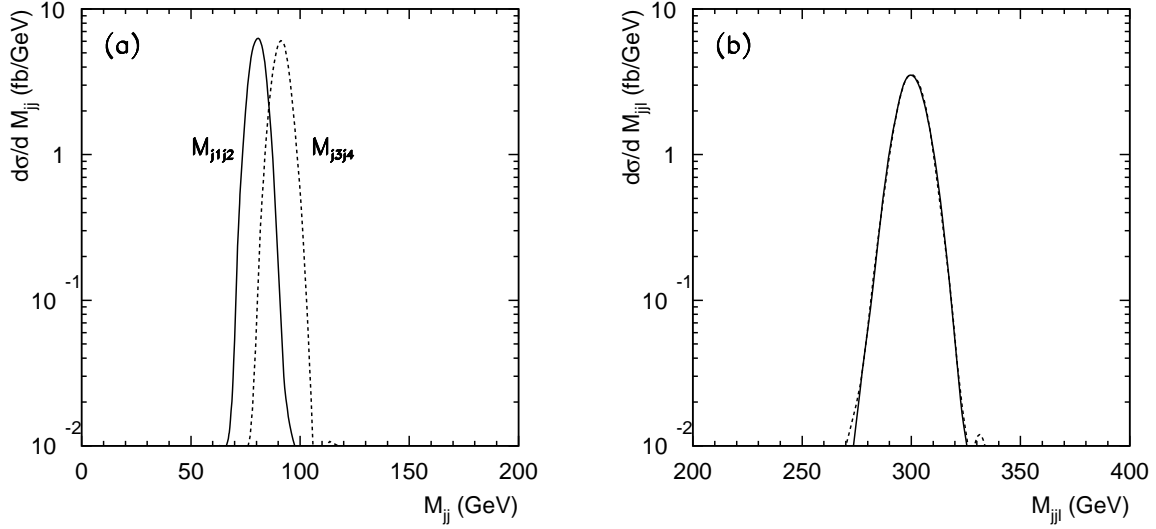


FIG. 17: Reconstructed invariant mass of $M(j_1j_2)$, $M(j_3j_4)$ (a) and $M(\ell_1j_1j_2)$, $M(\ell_2j_3j_4)$ (b) for $\ell^\pm\ell^\pm jjjj$ production, with a E mass of 300 GeV.

$$\text{BR}(E^+ E^- (E^\pm N) \rightarrow \ell\ell ZZ(\ell\ell ZW)) \approx \begin{cases} (23\%)^2 & \text{for NH : } (\mu^\pm + \tau^\pm)(\mu^\pm + \tau^\pm)ZZ(ZW), \\ (13\%)^2 & \text{for IH : } e^\pm e^\pm ZZ(ZW), \\ (17\%)^2 & \text{for QD : } (e^\pm + \mu^\pm + \tau^\pm)(e^\pm + \mu^\pm + \tau^\pm)ZZ(ZW), \end{cases} \quad (45)$$

supporting statement above. These predictions are the consequence from the neutrino oscillation experiments and are subject to be tested at the LHC to confirm the seesaw theory. However for the more general situation Case II when heavy neutrinos are not degenerate, no such information can be extracted since the correlation between the BR and light neutrino mass patterns is not strong.

We would like to comment that even for the complicated Case II, interesting information about the model can still be extracted. As pointed out earlier that using information on the neutrino mass pattern from other experiments and the sizes of elements in V_{LN} from analysis here, one may be able to obtain more information about the model parameters such as the angles w_{ij} and the Majorana phases.

VI. SUMMARY

We have studied the properties of heavy $SU(2)_L$ triplet lepton in Type III seesaw model and also their signatures at the LHC for small mixing solution between light and heavy leptons. The small mixing solution

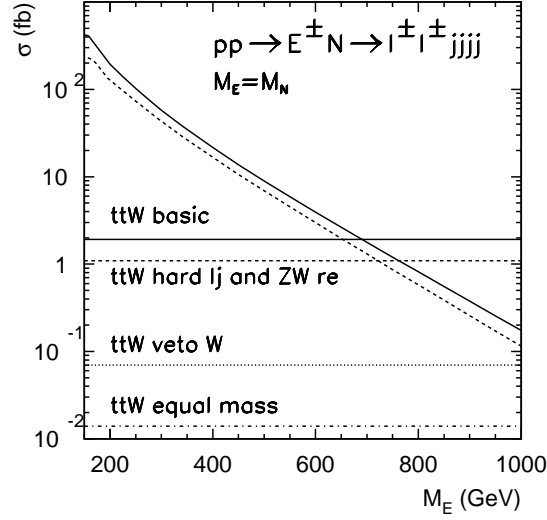


FIG. 18: Total cross section for $E^\pm N$ production after the basic cuts (solid) and all cuts (dashed) and the leading $t\bar{t}W^\pm$ background after all cuts.

is characterized by the fact that in the limit that the light neutrino masses go to zero, the mixing also goes to zero. The smallness of light neutrino masses then leads to the fact that the total decay widths of heavy leptons are small. With such small decay widths, although not considered as long-lived for large triplet mass, the heavy lepton decays could lead to a visible displaced vertex in the detector at the LHC. This displaced vertex can be observed through E and N reconstructions. We summarize our main results with small mixing in the following:

- To a good approximation, the couplings of light charged lepton and heavy triplet leptons V_{lN} to Z , W and H^0 bosons in Eq. 17 can be expressed with measurable neutrino mass and mixing through Eq. 18 with three unknown complex parameters w_{ij} in a 3×3 orthogonal matrix given in Eq. 25. This allowed us to study the correlation between the decays of heavy triplet leptons, light neutrino masses and mixing and model parameters. With real w_{ij} , the mixing between light and heavy is small which leads to displaced vertex at the LHC for heavy leptons decays if produced.
- Using the relation in Eq. 18, we have tried to study possible correlation in neutrino mass hierarchy and heavy lepton decays with real w_{ij} . We find that only in certain limited cases, for example Case I studied in this paper, the correlation is strong. The study of heavy lepton productions and decays at the LHC may help to determine the neutrino mass hierarchy. For the more general situation Case II when heavy neutrinos are not degenerate, no such information can be extracted because the

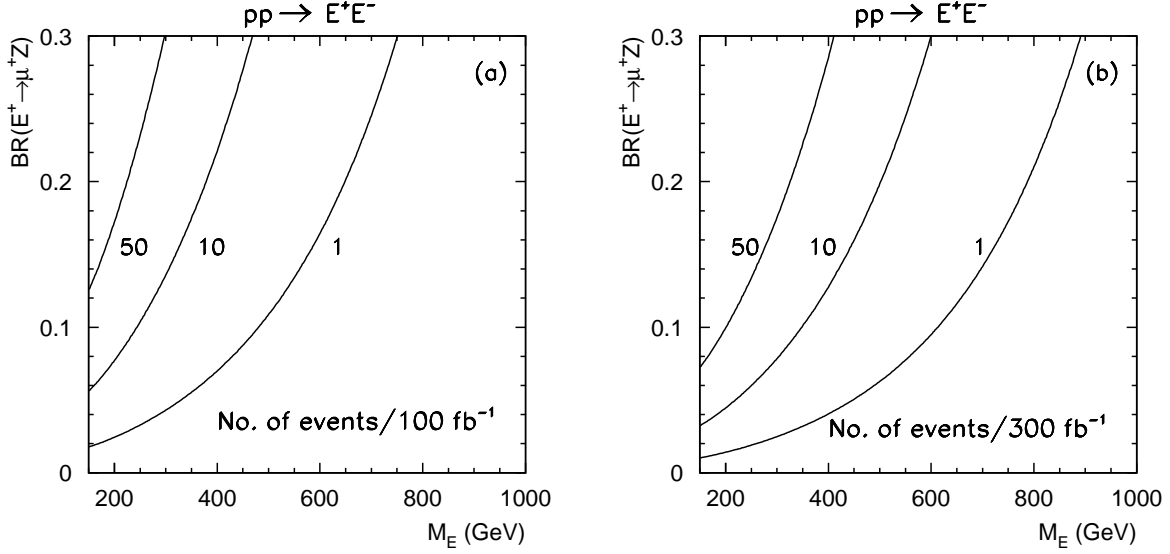


FIG. 19: Event contours in the BR - M_E plane at the LHC with integrated luminosity 100 fb^{-1} (a) and 300 fb^{-1} (b) for $E^+ E^- \rightarrow \mu^+ Z \mu^- Z \rightarrow \mu^+ \mu^+ \mu^- \mu^- jj$, including all the judicious cuts described in the early section.

correlation is weak. However, even for this case interesting information about the model can still be extracted. If in the future the neutrino mass pattern is determined from other experiments and the sizes of elements in V_{lN} from analysis of heavy lepton productions and decays at the LHC, one may be able to obtain more information about the model parameters such as the angles w_{ij} and the Majorana phases Φ_i .

- We have studied production and detection of heavy triplet leptons at LHC with judicious cuts to reduce SM background to see how large the seesaw scale can be reach at the LHC. The associated production $E^\pm N$ is crucial to identify the quantum numbers of the triplet leptons and to distinguish between the neutrino mass hierarchies. Even with only the cleanest channels $\mu^\pm \mu^\pm + \text{jets}$, the signal observability can reach about $M_E \lesssim 1 \text{ TeV}$ for 100 fb^{-1} luminosity and $M_E \lesssim 1.2 \text{ TeV}$ for 300 fb^{-1} luminosity.
- Although the rate of pair production $E^+ E^-$ is smaller than $E^\pm N$, we demonstrated that besides the clean 4-lepton channels from e, μ , the τ final state can be effectively reconstructed as well. Even with only the cleanest channels $\mu^+ \mu^+ \mu^- \mu^- + \text{jets}$, the signal observability can reach $M_E \lesssim 0.8 \text{ TeV}$ for 100 fb^{-1} luminosity and $M_E \lesssim 0.9 \text{ TeV}$ for 300 fb^{-1} luminosity.

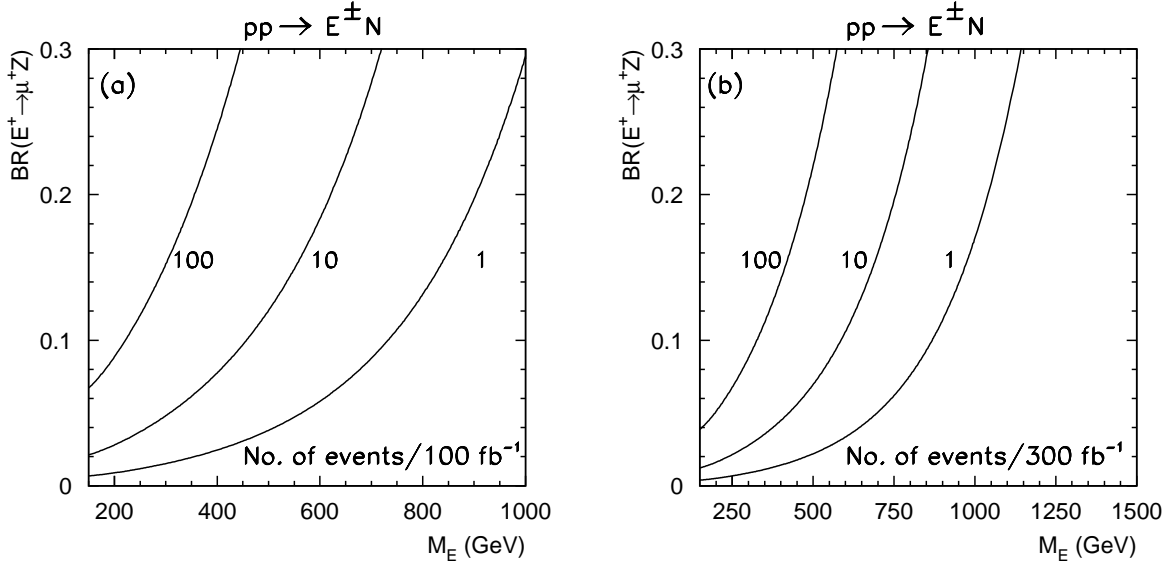


FIG. 20: Event contours in the BR - M_E plane at the LHC with integrated luminosity 100 fb^{-1} (a) and 300 fb^{-1} (b) for $E^\pm N \rightarrow \mu^\pm Z \mu^\pm W^\mp \rightarrow \mu^\pm \mu^\pm jjjj$, including all the judicious cuts described in the early section.

If Nature does use low scale, as low as 1 TeV, to facilitate seesaw mechanism, there will be a lot of surprises to come soon after LHC will be in full operation. We urge our experimentalists to carry out searches for low scale seesaw effects.

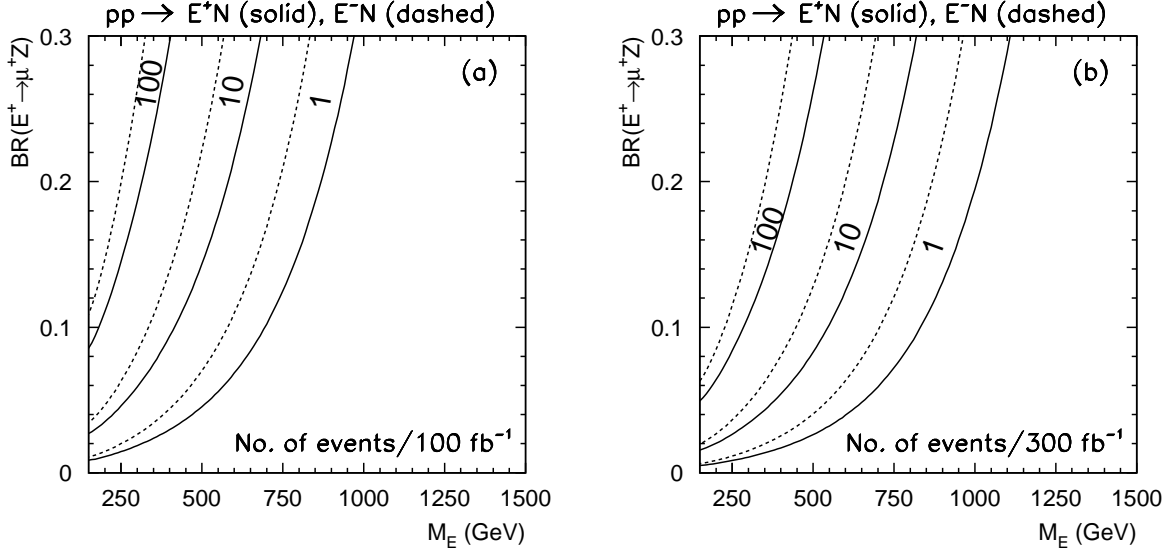


FIG. 21: Event contours in the $BR-M_E$ plane at the LHC with integrated luminosity 100 fb^{-1} (a) and 300 fb^{-1} (b) for $E^+ N \rightarrow \mu^+ Z \mu^+ W^- \rightarrow \mu^+ \mu^+ jjjj$ (solid line) and $E^- N \rightarrow \mu^- Z \mu^- W^+ \rightarrow \mu^- \mu^- jjjj$ (dashed line), including all the judicious cuts described in the early section.

Acknowledgment

XGH was supported in part by the NSC and NCTS. We acknowledge Tao Han for providing his Fortran codes HANLIB for our calculations. T. Li would like to thank Tao Han and Pavel Fileviez Pérez for helpful discussions.

APPENDIX A: DERIVATION OF EQUATION 13

To derive Eq. 13, we need to have some detailed relation of the block matrices in the unitary matrices U_0 and $U_{L,R}$. For U_0 , we have

$$\begin{aligned} U_{0\nu\nu}U_{0\nu\nu}^\dagger + U_{0\nu\Sigma}U_{0\nu\Sigma}^\dagger &= U_{0\Sigma\nu}U_{0\Sigma\nu}^\dagger + U_{0\Sigma\Sigma}U_{0\Sigma\Sigma}^\dagger = 1, \\ U_{0\nu\nu}^\dagger U_{0\nu\nu} + U_{0\Sigma\nu}^\dagger U_{0\Sigma\nu} &= U_{0\nu\Sigma}^\dagger U_{0\nu\Sigma} + U_{0\Sigma\Sigma}^\dagger U_{0\Sigma\Sigma} = 1, \\ U_{0\nu\nu}U_{0\Sigma\nu}^\dagger + U_{0\nu\Sigma}U_{0\Sigma\Sigma}^\dagger &= U_{0\nu\nu}^\dagger U_{0\nu\Sigma} + U_{0\Sigma\nu}^\dagger U_{0\Sigma\Sigma} = 0. \end{aligned} \quad (\text{A1})$$

From neutrino mass matrix diagonalization, we have

$$U_0^\dagger \begin{pmatrix} 0 & Y_\Sigma^\dagger v/\sqrt{2} \\ Y_\Sigma^* v/\sqrt{2} & M_\Sigma^* \end{pmatrix} U_0^* = \begin{pmatrix} m_\nu^{diag} & 0 \\ 0 & M_{\Sigma N}^{diag} \end{pmatrix}, \quad (\text{A2})$$

and

$$\begin{aligned} U_{0\Sigma\nu}^\dagger Y_\Sigma^* v / \sqrt{2} &= m_\nu^{diag} U_{0\nu\nu}^T, \quad Y_\Sigma^\dagger v U_{0\Sigma\Sigma}^* / \sqrt{2} = U_{0\nu\Sigma} M_{\Sigma N}^{diag}, \\ U_{0\nu\nu}^\dagger Y_\Sigma^\dagger v / \sqrt{2} + U_{0\Sigma\nu}^\dagger M_\Sigma^* &= m_\nu^{diag} U_{0\Sigma\nu}^T, \quad Y_\Sigma^* v U_{0\nu\Sigma}^* / \sqrt{2} + M_\Sigma^* U_{0\Sigma\Sigma}^* = U_{0\Sigma\Sigma} M_{\Sigma N}^{diag}. \end{aligned} \quad (A3)$$

For $U_{L,R}$, we have

$$\begin{aligned} U_{L,Rll} U_{L,Rll}^\dagger + U_{L,Rl\Psi} U_{L,Rl\Psi}^\dagger &= U_{L,R\Psi l} U_{L,R\Psi l}^\dagger + U_{L,R\Psi\Psi} U_{L,R\Psi\Psi}^\dagger = 1, \\ U_{L,Rll}^\dagger U_{L,Rll} + U_{L,R\Psi l}^\dagger U_{L,R\Psi l} &= U_{L,Rl\Psi}^\dagger U_{L,Rl\Psi} + U_{L,R\Psi\Psi}^\dagger U_{L,R\Psi\Psi} = 1, \\ U_{L,Rll} U_{L,R\Psi l}^\dagger + U_{L,Rl\Psi} U_{L,R\Psi\Psi}^\dagger &= U_{L,Rll}^\dagger U_{L,Rl\Psi} + U_{L,R\Psi l}^\dagger U_{L,R\Psi\Psi} = 0. \end{aligned} \quad (A4)$$

From charged lepton mass matrix diagonalization, we have

$$U_L^\dagger \begin{pmatrix} m_l^\dagger & Y_\Sigma^\dagger v \\ 0 & M_\Sigma^\dagger \end{pmatrix} U_R = \begin{pmatrix} m_l^{diag} & 0 \\ 0 & M_{\Sigma C}^{diag} \end{pmatrix} \quad (A5)$$

and

$$\begin{aligned} U_{Lll}^\dagger m_l^\dagger &= m_l^{diag} U_{Rll}^\dagger, \quad M_\Sigma^\dagger U_{R\Psi\Psi} = U_{L\Psi\Psi} M_{\Sigma C}^{diag}, \\ U_{R\Psi l}^\dagger M_\Sigma &= m_l^{diag} U_{L\Psi l}^\dagger, \quad m_l U_{Ll\Psi} = U_{Rl\Psi} M_{\Sigma C}^{diag}, \\ U_{Rll}^\dagger m_l + U_{R\Psi l}^\dagger Y_\Sigma v &= m_l^{diag} U_{Lll}^\dagger, \quad Y_\Sigma v U_{Ll\Psi} + M_\Sigma U_{L\Psi\Psi} = U_{R\Psi\Psi} M_{\Sigma C}^{diag}, \\ U_{Lll}^\dagger Y_\Sigma^\dagger v + U_{L\Psi l}^\dagger M_\Sigma^\dagger &= m_l^{diag} U_{R\Psi l}^\dagger, \quad m_l^\dagger U_{Rl\Psi} + Y_\Sigma^\dagger v U_{R\Psi\Psi} = U_{Ll\Psi} M_{\Sigma C}^{diag}. \end{aligned} \quad (A6)$$

Combining the above relations and the definition of $V_{l\Sigma}^L$, and using the approximation $M_{\Sigma N} = M_{\Sigma C} = M_\Sigma$, we obtain

$$V_{l\Sigma}^L = U_{Lll}^\dagger U_{0\nu\Sigma} + \sqrt{2} U_{L\Psi l}^\dagger U_{0\Sigma\Sigma}, \quad (A7)$$

which leads to

$$V_{l\Sigma}^L = V_{PMNS} U_{0\nu\nu}^\dagger U_{0\nu\Sigma} + \sqrt{2} U_{L\Psi l}^\dagger U_{0\Sigma\Sigma} + V_{l\Sigma}^L U_{0\nu\Sigma}^\dagger U_{0\nu\Sigma}. \quad (A8)$$

Then we have

$$V_{l\Sigma}^* M_{\Sigma N}^{diag} U_{0\nu\Sigma}^\dagger U_{Lll} = -V_{PMNS}^* m_\nu^{diag} U_{0\nu\nu}^\dagger U_{Lll} + \sqrt{2} U_{L\Psi l}^T Y_\Sigma v \sqrt{2} U_{Lll}. \quad (A9)$$

From the definition of $V_{l\Sigma}^L$ we can also get

$$V_{l\Sigma}^L = V_{PMNS} U_{0\Sigma\nu}^\dagger U_{0\Sigma\Sigma} + U_{Lll}^\dagger U_{0\nu\Sigma} + V_{l\Sigma}^L U_{0\Sigma\Sigma}^\dagger U_{0\Sigma\Sigma} \quad (A10)$$

which leads to

$$\begin{aligned} V_{l\Sigma}^{L*} M_{\Sigma N}^{diag} U_{0\Sigma\Sigma}^\dagger U_{L\Psi l} &= -V_{PMNS}^* m_\nu^{diag} U_{0\Sigma\nu}^\dagger U_{L\Psi l} + V_{l\Sigma}^{L*} U_{0\Sigma\Sigma}^T M_\Sigma^T U_{L\Psi l} \\ &+ V_{PMNS}^* U_{0\Sigma\nu}^T M_\Sigma U_{L\Psi l} + U_{Ll}^T Y_\Sigma^T v U_{L\Psi l} / \sqrt{2} . \end{aligned} \quad (A11)$$

Combining Eqs. A9 and A11, we finally obtain

$$\begin{aligned} V_{l\Sigma}^{L*} M_{\Sigma N}^{diag} V_{l\Sigma}^{L\dagger} &= -V_{PMNS}^* m_\nu^{diag} V_{PMNS}^\dagger + V_{l\Sigma}^{L*} U_{0\Sigma\Sigma}^T M_\Sigma^T U_{L\Psi l} \sqrt{2} + V_{PMNS}^* U_{0\Sigma\nu}^T M_\Sigma U_{L\Psi l} \sqrt{2} \\ &+ U_{Ll}^T Y_\Sigma^T v U_{L\Psi l} + U_{L\Psi l}^T Y_\Sigma v U_{Ll} \\ &= -V_{PMNS}^* m_\nu^{diag} V_{PMNS}^\dagger + m_l^{diag} U_{R\Psi l}^T U_{L\Psi l} + U_{L\Psi l}^T U_{R\Psi l} m_l^{diag} . \end{aligned} \quad (A12)$$

APPENDIX B: EXPLICIT EXPRESSIONS OF V_{lN} FOR CASE II

From Eq. 18 we can write V_{lN} explicitly as

$$V_{lN} = i V_{PMNS} (m_\nu^{diag})^{1/2} \Omega (M_N^{diag})^{-1/2} , \quad (B1)$$

where Ω is matrix which satisfies $\Omega \Omega^T = 1$. It can be parameterized as

$$\Omega(w_{21}, w_{31}, w_{32}) = R_{12}(w_{21}) R_{13}(w_{31}) R_{23}(w_{32}) , \quad (B2)$$

with

$$R_{12} = \begin{pmatrix} cw_{21} & -sw_{21} & 0 \\ sw_{21} & cw_{21} & 0 \\ 0 & 0 & 1 \end{pmatrix} , \quad R_{13} = \begin{pmatrix} cw_{31} & 0 & -sw_{31} \\ 0 & 1 & 0 \\ sw_{31} & 0 & cw_{31} \end{pmatrix} , \quad R_{23} = \begin{pmatrix} 1 & 0 & 0 \\ 0 & cw_{32} & -sw_{32} \\ 0 & sw_{32} & cw_{32} \end{pmatrix} ,$$

where $sw_{ij} = \sin(w_{ij})$ and $cos(w_{ij})$.

The couplings V_{lN} for different charged lepton and heavy neutrino flavors are

$$\begin{aligned} -i V_{lN}^{e1} \sqrt{M_1} &= \sqrt{m_2} c_{13} s_{12} s w_{21} c w_{31} + \sqrt{m_1} c_{12} c_{13} c w_{21} c w_{31} e^{i\Phi_1/2} + \sqrt{m_3} s_{13} s w_{31} e^{i(\Phi_2/2-\delta)} , \\ -i V_{lN}^{\mu 1} \sqrt{M_1} &= \sqrt{m_2} (c_{12} c_{23} - s_{12} s_{13} s_{23} e^{i\delta}) s w_{21} c w_{31} \\ &+ \sqrt{m_1} (-s_{12} c_{23} - c_{12} s_{13} s_{23} e^{i\delta}) c w_{21} c w_{31} e^{i\Phi_1/2} + \sqrt{m_3} c_{13} s_{23} s w_{31} e^{i\Phi_2/2} , \\ -i V_{lN}^{\tau 1} \sqrt{M_1} &= \sqrt{m_2} (-c_{12} s_{23} - s_{12} s_{13} c_{23} e^{i\delta}) s w_{21} c w_{31} \\ &+ \sqrt{m_1} (s_{12} s_{23} - c_{12} s_{13} c_{23} e^{i\delta}) c w_{21} c w_{31} e^{i\Phi_1/2} + \sqrt{m_3} c_{13} c_{23} s w_{31} e^{i\Phi_2/2} , \end{aligned} \quad (B3)$$

$$\begin{aligned}
-iV_{lN}^{e2}\sqrt{M_2} &= \sqrt{m_2}c_{13}s_{12}(-sw_{21}sw_{31}sw_{32} + cw_{21}cw_{32}) , \\
&+ \sqrt{m_1}c_{12}c_{13}(-sw_{31}sw_{32}cw_{21} - sw_{21}cw_{32})e^{i\Phi_1/2} + \sqrt{m_3}s_{13}sw_{32}cw_{31}e^{i(\Phi_2/2-\delta)} , \\
-iV_{lN}^{\mu 2}\sqrt{M_2} &= \sqrt{m_2}(c_{12}c_{23} - s_{12}s_{13}s_{23}e^{i\delta})(-sw_{21}sw_{31}sw_{32} + cw_{21}cw_{32}) , \\
&+ \sqrt{m_1}(-s_{12}c_{23} - c_{12}s_{13}s_{23}e^{i\delta})(-sw_{32}sw_{31}cw_{21} - sw_{21}cw_{32})e^{i\Phi_1/2} \\
&+ \sqrt{m_3}c_{13}s_{23}sw_{32}cw_{31}e^{i\Phi_2/2} , \\
-iV_{lN}^{\tau 2}\sqrt{M_2} &= \sqrt{m_2}(-c_{12}s_{23} - s_{12}s_{13}c_{23}e^{i\delta})(-sw_{21}sw_{31}sw_{32} + cw_{21}cw_{32}) \\
&+ \sqrt{m_1}(s_{12}s_{23} - c_{12}s_{13}c_{23}e^{i\delta})(-sw_{32}sw_{31}cw_{21} - sw_{21}cw_{32})e^{i\Phi_1/2} \\
&+ \sqrt{m_3}c_{13}c_{23}sw_{32}cw_{31}e^{i\Phi_2/2} , \tag{B4}
\end{aligned}$$

$$\begin{aligned}
-iV_{lN}^{e3}\sqrt{M_3} &= \sqrt{m_2}c_{13}s_{12}(-sw_{32}cw_{21} - sw_{21}sw_{31}cw_{32}) , \\
&+ \sqrt{m_1}c_{12}c_{13}(sw_{21}sw_{32} - sw_{31}cw_{21}cw_{32})e^{i\Phi_1/2} \\
&+ \sqrt{m_3}s_{13}cw_{31}cw_{32}e^{i(\Phi_2/2-\delta)} , \\
-iV_{lN}^{\mu 3}\sqrt{M_3} &= \sqrt{m_2}(c_{12}c_{23} - s_{12}s_{13}s_{23}e^{i\delta})(-sw_{32}cw_{21} - sw_{21}sw_{31}cw_{32}) \\
&+ \sqrt{m_1}(-s_{12}c_{23} - c_{12}s_{13}s_{23}e^{i\delta})(sw_{32}sw_{21} - sw_{31}cw_{21}cw_{32})e^{i\Phi_1/2} \\
&+ \sqrt{m_3}c_{13}s_{23}cw_{31}cw_{32}e^{i\Phi_2/2} , \\
-iV_{lN}^{\tau 3}\sqrt{M_3} &= \sqrt{m_2}(-c_{12}s_{23} - s_{12}s_{13}c_{23}e^{i\delta})(-sw_{32}cw_{21} - sw_{21}sw_{31}cw_{32}) \\
&+ \sqrt{m_1}(s_{12}s_{23} - c_{12}s_{13}c_{23}e^{i\delta})(sw_{32}sw_{21} - sw_{31}cw_{21}cw_{32})e^{i\Phi_1/2} \\
&+ \sqrt{m_3}c_{13}c_{23}cw_{31}cw_{32}e^{i\Phi_2/2} . \tag{B5}
\end{aligned}$$

Note that Ω is only required to satisfy $\Omega\Omega^T = 1$, the angles w_{ij} can take complex values. In principle, the elements in Ω is unbounded. For example taking w_{ij} to be imaginary and arbitrarily large will lead to large light and heavy neutrino mixing. Since we are only interested in small mixing with element in V_{lN} of order $\sqrt{m_\nu/M_N}$, we will consider in the main text that the element in Ω to be real numbers by restricting the ranges of w_{ij} to be $0 \leq w_{ij} \leq 2\pi$. In this case the above general solution belongs to the small mixing solution. In the limit the light neutrino masses go to zero, all elements in V_{lN} is guaranteed go to zero. Also

these elements are of order $(m_\nu/M_{\nu_R})^{1/2}$.

-
- [1] P. Minkowski, Phys. Lett. B **67**, 421 (1977); T. Yanagida, in *Workshop on Unified Theories*, KEK report 79-18 p.95 (1979); M. Gell-Mann, P. Ramond, R. Slansky, in *Supergravity* (North Holland, Amsterdam, 1979) eds. P. van Nieuwenhuizen, D. Freedman, p.315; S. L. Glashow, in *1979 Cargese Summer Institute on Quarks and Leptons* (Plenum Press, New York, 1980) eds. M. Levy, J.-L. Basdevant, D. Speiser, J. Weyers, R. Gastmans and M. Jacobs, p.687; R. Barbieri, D. V. Nanopoulos, G. Morchio and F. Strocchi, Phys. Lett. B **90**, 91 (1980); R. N. Mohapatra and G. Senjanovic, Phys. Rev. Lett. **44**, 912 (1980); G. Lazarides, Q. Shafi and C. Wetterich, Nucl. Phys. B **181**, 287 (1981).
 - [2] W. Konetschny and W. Kummer, Phys. Lett. B **70**, 433 (1977); T. P. Cheng and L. F. Li, Phys. Rev. D **22**, 2860 (1980); G. Lazarides, Q. Shafi and C. Wetterich, Nucl. Phys. B **181**, 287 (1981); J. Schechter and J. W. F. Valle, Phys. Rev. D **22**, 2227 (1980); R. N. Mohapatra and G. Senjanovic, Phys. Rev. D **23**, 165 (1981).
 - [3] R. Foot, H. Lew, X. G. He and G. C. Joshi, Z. Phys. C **44**, 441 (1989).
 - [4] For recent reviews on neutrino physics, see *e.g.*, V. Barger, D. Marfatia, and K. Whisnant, Int. J. Mod. Phys. **E12**, 569 (2003); B. Kayser, p. 145 of the Review of Particle Physics, Phys. Lett. **B592**, 1 (2004); M. C. Gonzalez-Garcia and M. Maltoni, arXiv:0704.1800 [hep-ph]; R. N. Mohapatra and A. Y. Smirnov, Ann. Rev. Nucl. Part. Sci. **56** (2006) 569 [arXiv:hep-ph/0603118]; A. Strumia and F. Vissani, arXiv:hep-ph/0606054; Z. Z. Xing, *Plenary talk at 34th International Conference on High Energy Physics* (ICHEP 2008, Philadelphia, Pennsylvania, 30 Jul - 5 Aug 2008), Int. J. Mod. Phys. **A23** (2008) 4255.
 - [5] W. Y. Keung and G. Senjanović, Phys. Rev. Lett. **50** (1983) 1427; D. A. Dicus, D. D. Karatas and P. Roy, Phys. Rev. D **44** (1991) 2033; A. Datta, M. Guchait and A. Pilaftsis, Phys. Rev. D **50** (1994) 3195; F. M. L. Almeida, Y. D. A. Coutinho, J. A. Martins Simoes and M. A. B. do Vale, Phys. Rev. D **62** (2000) 075004; O. Panella, M. Cannoni, C. Carimalo and Y. N. Srivastava, Phys. Rev. D **65** (2002) 035005.
 - [6] T. Han and B. Zhang, Phys. Rev. Lett. **97**, 171804 (2006); A. Atre, T. Han, S. Pascoli, B. Zhang, arXiv:0901.3589 [hep-ph]
 - [7] For a comparison for different colliders, see *e.g.*, F. del Aguila, J. A. Aguilar-Saavedra and R. Pittau, J. Phys. Conf. Ser. **53**, 506 (2006) [arXiv:hep-ph/0606198]; F. del Aguila, J. A. Aguilar-Saavedra and R. Pittau, JHEP **0710**, 047 (2007) [arXiv:hep-ph/0703261]; J. Kersten and A. Y. Smirnov, Phys. Rev. D **76**, 073005 (2007) [arXiv:0705.3221 [hep-ph]]; S. Bar-Shalom, G. Eilam, T. Han and A. Soni, arXiv:0803.2835 [hep-ph].
 - [8] P. F. Pérez, T. Han and T. Li, arXiv:0907.4186 [hep-ph].
 - [9] E. J. Chun, K. Y. Lee and S. C. Park, Phys. Lett. B **566** (2003) 142 [arXiv:hep-ph/0304069]; T. Han, H. E. Logan, B. Mukhopadhyaya and R. Srikanth, Phys. Rev. D **72**, 053007 (2005) [arXiv:hep-ph/0505260]; C. S. Chen, C. Q. Geng, J. N. Ng and J. M. S. Wu, JHEP **0708** (2007) 022 [arXiv:0706.1964 [hep-ph]]; A. Hektor, M. Kadastik, M. Muntel, M. Raidal and L. Rebane, Nucl. Phys. B **787**, 198 (2007) [arXiv:0705.1495 [hep-ph]]; T. Han, B. Mukhopadhyaya, Z. Si and K. Wang, Phys. Rev. D **76**, 075013 (2007) [arXiv:0706.0441 [hep-ph]];

- J. Garayoa and T. Schwetz, arXiv:0712.1453 [hep-ph]; M. Kadastik, M. Raidal and L. Rebane, arXiv:0712.3912 [hep-ph]; A. G. Akeroyd, M. Aoki and H. Sugiyama, arXiv:0712.4019 [hep-ph]; W. Chao, S. Luo, Z. Z. Xing and S. Zhou, Phys. Rev. D **77**, 016001 (2008) [arXiv:0709.1069 [hep-ph]]; W. Chao, Z. G. Si, Z. Z. Xing and S. Zhou, arXiv:0804.1265 [hep-ph].
- [10] P. F. Pérez, T. Han, G. Y. Huang, T. Li and K. Wang, Phys. Rev. **D78** (2008) 071301; Phys. Rev. **D78** (2008) 015018; P. F. Pérez, T. Han, T. Li and M. J. Ramsey-Musolf, arXiv:0810.4138 [hep-ph].
- [11] R. Franceschini, T. Hambye and A. Strumia, Phys. Rev. D **78**, 033002 (2008) [arXiv:0805.1613 [hep-ph]].
- [12] B. Bajc, M. Nemevsek and G. Senjanovic, Phys. Rev. D **76**, 055011 (2007) [arXiv:hep-ph/0703080]; P. F. Pérez, arXiv:0809.1202 [hep-ph].
- [13] F. d. Aguila, J. A. Aguilar-Saavedra, arXiv:0808.2468 [hep-ph]; J. A. Aguilar-Saavedra, arXiv:0905.2221 [hep-ph].
- [14] D. Wyler and L. Wolfenstein, Nucl. Phys. **B218**, 205(1983); R. N. Mohapatra and J. W. F. Valle, Phys. Lett. B **177**, 47 (1986); E. Ma, Phys. Lett. **B191**, 287(1987).
- [15] W. Buchmuller and D. Wyler, Phys. Lett. B **249**, 458 (1990); A. Pilaftsis, Phys. Rev. Lett. **95**, 081602 (2005) [arXiv:hep-ph/0408103]; J. Kersten and A.Y. Smirnov, Phys. Rev. D **76**, 073005 (2007) [arXiv:0705.3221 [hep-ph]]; E. Ma, arXiv:0904.1580 [hep-ph]; Z.Z. Xing, arXiv:0905.3903 [hep-ph]; M. Malinsky, T. Ohlsson, H. Zhang, arXiv:0903.1961 [hep-ph]; M. Malinsky, T. Ohlsson, Z.Z Xing, H. Zhang, arXiv:0905.2889 [hep-ph]; X. G. He and E. Ma, arXiv:0907.2737 [hep-ph].
- [16] Xiao-Gang He, Sechul Oh, Jusak Tandean and Chung-Cheng Wen, arXiv:0907.1607 [hep-ph].
- [17] A. Arhrib, B. Bajc, D. K. Ghosh, T. Han, G. Y. Huang, I. Puljak and G. Senjanovic, arXiv:0904.2390 [hep-ph].
- [18] A. Abada, C. Biggio, F. Bonnet, M. B. Gavela, T. Hambye, Phys. Rev. **D78** (2008) 033007 [arXiv:0803.0481]; A. Abada, C. Biggio, F. Bonnet, M. B. Gavela and T. Hambye, JHEP **0712**, 061 (2007) [arXiv:0707.4058 [hep-ph]]; E. Fernandez-Martinez, M. B. Gavela, J. Lopez-Pavon and O. Yasuda, Phys. Lett. B **649**, 427 (2007) [arXiv:hep-ph/0703098]; X. G. He and S. Oh, arXiv:0902.4082 [hep-ph].
- [19] A. Arhrib, R. Benbrik and C. H. Chen, arXiv:0903.1553 [hep-ph]; C. Biggio, Phys. Lett. B **668**, 378 (2008) [arXiv:0806.2558 [hep-ph]]; W. Chao, arXiv:0806.0889 [hep-ph]; Y. Liao, J. Y. Liu and G. Z. Ning, arXiv:0902.1434 [hep-ph].
- [20] T. Hambye, Y. Lin, A. Notari, M. Papucci and A. Strumia, Nucl. Phys. B **695**, 169 (2004) [arXiv:hep-ph/0312203]; A. Strumia, Nucl. Phys. B **809**, 308 (2009) [arXiv:0806.1630 [hep-ph]]; S. Blanchet, arXiv:0807.1408 [hep-ph]; F. X. F. Josse-Michaux, arXiv:0809.4960 [hep-ph]; Shao-Long Chen and Xiao-Gang He, arXiv:0901.1264 [hep-ph]. F. Borzumati and T. Yamashita, arXiv:0903.2793 [hep-ph].
- [21] J. Chakraborty, A. Dighe, S. Goswami and S. Ray, arXiv:0812.2776 [hep-ph]; R. N. Mohapatra, N. Okada and H. B. Yu, Phys. Rev. D **78**, 075011 (2008) [arXiv:0807.4524 [hep-ph]]. M. Hirsch, S. Morisi and J. W. F. Valle, arXiv:0810.0121 [hep-ph]; E. Ma, arXiv:0810.5574 [hep-ph]; P. Fileviez Perez, Phys. Lett. B **654**, 189 (2007) [arXiv:hep-ph/0702287]; R. Adhikari, J. Erler and E. Ma, arXiv:0810.5547 [hep-ph]. I. Dorsner and P. Fileviez Perez, JHEP **0706**, 029 (2007) [arXiv:hep-ph/0612216]; B. Bajc and G. Senjanovic, JHEP **0708**, 014 (2007) [arXiv:hep-ph/0612029]; E. Ma and D. P. Roy, Nucl. Phys. B **644**, 290 (2002) [arXiv:hep-ph/0206150];

- E. Ma, Phys. Rev. D **66**, 037301 (2002) [arXiv:hep-ph/0204013]; E. Ma, Mod. Phys. Lett. A **17**, 535 (2002) [arXiv:hep-ph/0112232].
- [22] J. A. Casas and A. Ibarra, Nucl. Phys. **B618** (2001) 171.
- [23] T. Schwetz, M. Tortola and J. W. F. Valle, New J. Phys. **10** (2008) 113011 [arXiv:0808.2016 [hep-ph]].
- [24] G. L. Fogli, E. Lisi, A. Marrone, A. Melchiorri, A. Palazzo, A. M. Rotunno, P. Serra, J. Silk and A. Slosar, Phys. Rev. D **78** (2008) 033010.
- [25] C. Amsler et al. (Particle Data Group), Phys. Lett. **B667** (2008) 1.
- [26] F. del Aguila, J. d. Blas and M. P. Victoria, Phys. Rev. **D78** (2008) 013010.
- [27] CMS TDR: *CMS Physics: Technical Design Report V.2: Physics Performance*, CERN-LHCC-2006-021.